Cell Reports

Article

Tolerance to extracellular acidic pH facilitates tumor plasticity

Graphical abstract

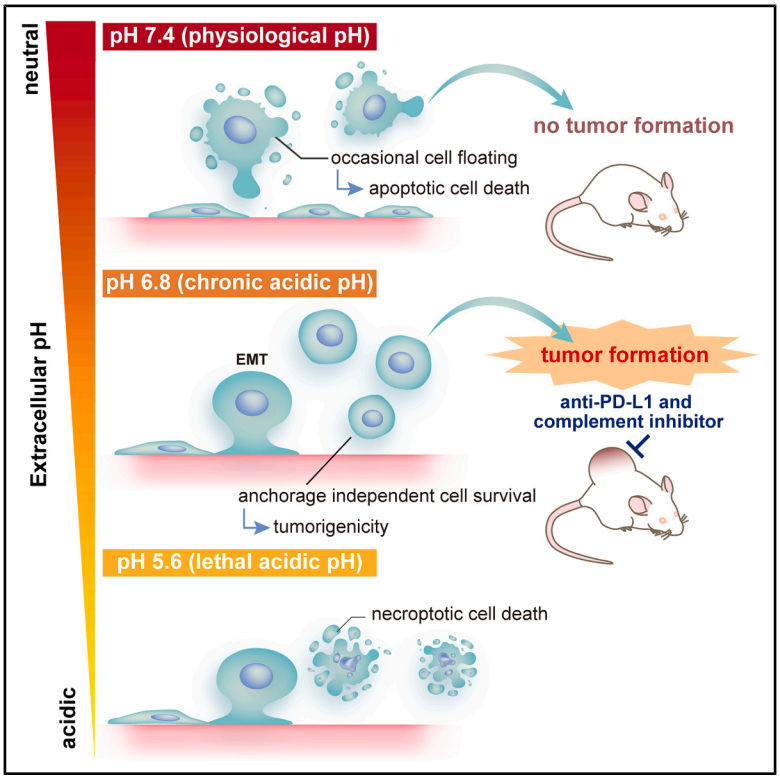

Highlights

- pH 5.6 induces necroptosis, whereas pH 6.8 induces anchorage-independent survival
- Cancer cells at pH 6.8 show enhanced tumor plasticity and tumorigenicity
- Chronic acidic pH promotes protumor immunity via the FAM129C-PIGR-complement axis
- Combination treatment with anti-complement/anti-PD-L1 suppresses acidic pH-adaptive tumors

Authors

Manami Hasegawa, Bo Xu, Keisuke Maeda, ..., Hideyuki Yanai, Nozomu Yachie, Tsuyoshi Osawa

Correspondence

osawa@onc.rcast.u-tokyo.ac.jp

In brief

Hasegawa et al. demonstrate that mild extracellular acidosis (pH 6.8) enables anchorage-independent survival and tumor plasticity, while severe acidosis (pH 5.6) induces necroptosis. Chronic acidic stress promotes protumor immunity via the FAM129C-PIGR-complement axis, uncovering a therapeutic vulnerability to combined complement and PD-L1 blockade.

Hasegawa et al., 2026, Cell Reports ■■, 117226
■■, 2026
https://doi.org/10.1016/j.celrep.2026.117226

CellPress

Cell Reports

CellPress
OPEN ACCESS

Article

Tolerance to extracellular acidic pH facilitates tumor plasticity

Manami Hasegawa,[1,2,16] Bo Xu,[1,3,16] Keisuke Maeda,[1] Motoaki Seki,[4] FeiFei Cai,[1] Runmei Cui,[5] Ritsuko Ando,[1] Suzuka Nakagawa,[6,7] Ayana Sakamoto,[1,8] Cayla Boycott,[1] Hiroyuki Yatabe,[2] Miyuki Nishida,[1] Ken Matsumoto,[1] Chisato Iwabuchi-Yoshida,[1] Sho Aki,[1,2] Kazuyuki Yamagata,[1] Rika Tsuchida,[1] Mami Takahashi,[9] Futoshi Kuribayashi,[10] Hiroyasu Kidoya,[11] Hiroshi Hirata,[12] Shingo Matsumoto,[12] Shinsuke Sando,[2,13] Hideyuki Yanai,[14] Nozomu Yachie,[15] and Tsuyoshi Osawa[1,2,5,17,*]

[1]Division of Nutriomics and Oncology, RCAST, Graduate School of Engineering, The University of Tokyo, Tokyo 153-8904, Japan
[2]Department of Chemistry and Biotechnology, Graduate School of Engineering, The University of Tokyo, Tokyo 113-8656, Japan
[3]School of Basic Medical Sciences of Zhengzhou University, 100 Kexue Avenue, Zhengzhou 450-0000, China
[4]Department of Molecular Oncology, Graduate School of Medicine, Chiba University, Chiba 260-8670, Japan
[5]Department of Biological Sciences, Graduate School of Science, The University of Tokyo, Tokyo 113-0033, Japan
[6]Max Delbrück Center for Molecular Medicine in the Helmholtz Association, 13125 Berlin, Germany
[7]Humboldt University of Berlin, 10099 Berlin, Germany
[8]Department of Chemistry, Carleton College, Northfield, MN 55057, USA
[9]Department of Pharmacology and Therapeutics, Fundamental Innovative Oncology Core, National Cancer Center Research Institute, Tokyo 104-0045, Japan
[10]School of Medicine, Department of Medicine, Kawasaki Medical School, 577 Matsushima, Kurashiki, Okayama 701-0192, Japan
[11]Department of Integrative Vascular Biology, Faculty of Medical Sciences, University of Fukui, Fukui 910-1193, Japan
[12]Division of Bioengineering and Bioinformatics, Faculty of Information Science and Technology, Hokkaido University, North 14, West 9, Kita-ku, Sapporo 060-0814, Japan
[13]Department of Bioengineering, Graduate School of Engineering, The University of Tokyo, Tokyo 113-8654, Japan
[14]Department of Inflammology, RCAST, The University of Tokyo, Tokyo 153-8904, Japan
[15]School of Biomedical Engineering, Faculty of Applied Science and Faculty of Medicine, The University of British Columbia, Vancouver, BC V6T 1Z3, Canada
[16]These authors contributed equally
[17]Lead contact
*Correspondence: osawa@onc.rcast.u-tokyo.ac.jp
https://doi.org/10.1016/j.celrep.2026.117226

SUMMARY

Cancer cells sustain glycolysis despite oxygen availability, creating an acidic microenvironment via proton and lactate export, but how they survive acid stress is unclear. We show that severe acidification (pH 5.6) induces necroptosis, whereas moderate acidity (pH 6.8) prevents death and enables anchorage-independent survival and tumor initiation. RNA sequencing of suspended cells at pH 6.8 revealed activation of respiratory chain complex and complement pathways, consistent with adaptation to this pH. A genome-wide CRISPR-Cas9 knockout screen in PANC1 cells under chronic acidity identified FAM129C as a regulator of acid tolerance and survival. In xenografts, FAM129C overexpression reduced PIGR expression, implicating this axis in tumor growth and immune infiltration. Anti-PD-L1 plus a complement inhibitor showed synergistic anti-tumor activity in PIGR-overexpressing tumors. Thus, acidic stress engages a pathway that allows cancer cells to evade necroptosis and promote tumor plasticity, providing potential avenues for therapeutic intervention targeting pH-dependent cell-death pathways.

INTRODUCTION

The tumor microenvironment significantly influences cancer progression and cellular plasticity through various stressors, including hypoxia, nutrient deprivation, and acidic extracellular pH (pHe).[1–3] Hypoxia has been extensively studied for its role in tumor development and its impact on cellular plasticity.[4] Hypoxia-inducible factors (HIFs) regulate genes associated with angiogenesis (VEGF-A), glucose metabolism (GLUT1 and PKM2), and cancer stemness[5–7] while promoting epithelial-to-mesenchymal transition (EMT) through transcription factors such as TWIST, SNAIL1/2, and ZEB1/2.[8] Although the role of hypoxia in regard to HIFs has been previously studied,[4] the influence of acidic pHe on cancer cell plasticity remains unclear. In acidic pH environments, oxidative phosphorylation is activated alongside glycolysis.[9] Within tumor tissues, pHe typically reaches approximately 6.8, resulting from enhanced proton and lactate secretion due to the Warburg and Pasteur effects, respectively.[10,11] Moreover, pH levels within tumors are heterogeneous, and the tumor core may reach a pH as acidic as

Please cite this article in press as: Hasegawa et al., Tolerance to extracellular acidic pH facilitates tumor plasticity, Cell Reports (2026), https://doi.org/10.1016/j.celrep.2026.117226

5.6.[12–15] Rather than merely being a downstream consequence of hypoxia, acidic pHe actively enhances metastatic potential by inducing angiogenic factors, including VEGF-A and interleukin-8 (IL-8).[16–19] The mechanism through which acidic pH induces cell death and survival remains unclear.[20] It has been reported that acidic pH induces caspase-dependent apoptosis in chondrocytes,[21] ferroptosis in breast cancer,[22] and pyroptosis in liver injury.[23] However, our previous research also demonstrated that an acidic pH environment promotes cell survival,[24,25] indicating the presence of complex adaptations to environmental stress.

There are distinct cellular responses to an acidic extracellular environment. An acidic pHe activates SREBP2 through nuclear translocation and enhances promoter binding, accompanied by intracellular acidification.[24] In tumor-associated neutrophils, extracellular acidification facilitates N1-acetylspermidine accumulation through SAT1 regulation, promoting tumor progression.[25] In pancreatic cancer, tumor acidosis has been shown to enhance stem-like properties and *in vivo* metastatic potential.[26] Acid adaptation of pancreatic organoids also increased viability and chemotherapy resistance.[27] Furthermore, acidic pH has been reported to confer reliance through oxidative phosphorylation (OXPHOS) genes in cancer cells.[9] Acidic environments also trigger comprehensive metabolic reprogramming, such as changes in glutamine metabolism and fatty acid utilization,[28] and induce p21-mediated senescence.[29] Metabolic reprogramming for adaptation to an acidic pH tumor microenvironment is a key cellular response. Despite the growing understanding of acute responses to acidic pHe, the mechanisms enabling long-term survival under chronic acidic conditions remain poorly characterized, partly because of the technical challenges in maintaining stable pH levels in culture systems. Most studies have focused on transient responses to acidic pH, leaving critical gaps in our understanding of cancer cell survival strategies in acidic tumor microenvironments. Here, we demonstrated that extreme acidification (pH 5.6) induces necroptotic cell death, while modulated acidity (typical acidity in tumor microenvironments, pH 6.8) triggers an alternative pathway to evade necroptotic cell death by transitioning into a floating state, enhancing respiratory activity, and inducing complement activation. Using genome-wide CRISPR knockout screening, we identified key regulators of cancer cell survival in chronically acidic environments and investigated their association with patient prognosis. Our findings reveal mechanisms of acid tolerance in cancer cells and suggest potential therapeutic strategies that target pH-dependent cell-death pathways. This study contributes to our fundamental understanding of cancer cell adaptation to acidic environments, a crucial step in the development of treatments targeting acid-resistant tumors.

RESULTS

Necroptosis was induced in cancer cells under extreme acidity

Acidic pH may induce cell death through caspase-dependent apoptosis,[21] ferroptosis,[22] and pyroptosis[23]; however, the mechanism of cell death induced by acidic pH has not been fully characterized. We investigated the correlation between clinical outcomes and the expression levels of functional executioner genes involved in different cell-death pathways (*MLKL* for necroptosis, *CASP3* for apoptosis, *GPX4* for ferroptosis, and *GSDMD* for pyroptosis). Although the expression levels of *MLKL*, *CASP3*, *GPX4*, and *GSDMD* were elevated in patients with cancer (Figure S1A), higher *GPX4* expression was associated with prolonged disease-free survival (DFS) (Figure 1A). Moreover, *CASP3*, *GPX4*, and *GSDMD* expression levels were significantly correlated with both overall survival (OS) and relapse-free survival in pancreatic adenocarcinoma (PAAD) (Figure S1B). However, expression of key genes in necroptosis (*RIPK1*, *RIPK3*, *MLKL*, *FADD*, *TNFR1*, and *TRADD*), apoptosis (*BAX*, *BAK*, *CYCS*, *CASP9*, *CASP3*, and *TP53*), ferroptosis (*GPX4*, *SLC7A11*, *ACSL4*, *ALOX15*, *TFRC*, and *FTH1*), and pyroptosis (*CASP1*, *GSDMD*, *NLRP3*, *IL-1B*, *CASP4*, and *ASC*) was associated with reduced OS in patients with pancreatic cancer (Figure S1C), indicating a correlation of cell-death pathways with cancer progression and malignancy.

Recent high-resolution, MRI-based *in vivo* pH imaging studies have reported localized tumor regions in which the pHe approaches 5.6.[12–15] We therefore monitored pH within pancreatic tumor xenografts (MIA-PaCa2 and SU86.86) in our system using electron paramagnetic resonance (EPR) and found regions with pH values as low as ~6.0 (Figure S1D). Moreover, relative to the tumor periphery, the core exhibited more hypoxic and acidic regions (Figures S1D–S1H).

Therefore, we investigated the mechanism underlying cell death induced by acidic conditions (pH 5.6 and 6.8) in cancer cells. Live-cell imaging using calcein AM staining revealed that MIA-PaCa2 cells exposed to extremely acidic conditions (pH 5.6) exhibited membrane rupture within 6 h (Figure 1B). This cellular damage was rarely observed under moderately acidic (pH 6.8) or neutral (pH 7.4) conditions (Figures 1B and S2A). Quantitative assessment of membrane destruction using lactate dehydrogenase (LDH) release assays in multiple cancer cells (PANC1, MIA-PaCa2, and HeLa) demonstrated significant cellular content release specifically under pH 5.6 conditions (Figure 1C), corresponding with substantial reduction in cell viability (Figure 1D).

We examined the executioner markers for various programmed cell-death mechanisms to elucidate the cell-death pathways induced under acidic conditions. While markers for apoptosis (caspase-3), ferroptosis (GPX4), and pyroptosis (GSDMD) showed no significant changes (Figures 1E, 1F, and S2B), we observed marked increases in the phosphorylation of necroptotic proteins RIP1 and MLKL, specifically at pH 5.6, in both PANC1 and MIA-PaCa2 cells (Figures 1E and 1F). The predominant involvement of necroptosis was further confirmed using the RIP1 inhibitor, necrostatin-1 (Nec1), which significantly reduced LDH release (Figure 1G) and improved cell viability (Figure 1H) at pH 5.6. Notably, prolonged treatment with multiple cell-death inhibitors (necroptosis, Nec1; apoptosis, zVAD-FMK; and ferroptosis, ferrostatin-1) under moderately acidic conditions (pH 6.8) did not affect cell proliferation (Figure S2C). Furthermore, MLKL-positive necroptosis was induced in the tumor core *in vivo* (Figures S2D and S2E). These findings suggest that necroptosis observed at pH 5.6 may not occur at pH 7.4 or pH 6.8.

Please cite this article in press as: Hasegawa et al., Tolerance to extracellular acidic pH facilitates tumor plasticity, Cell Reports (2026), https://doi.org/10.1016/j.celrep.2026.117226

CellPress
OPEN ACCESS

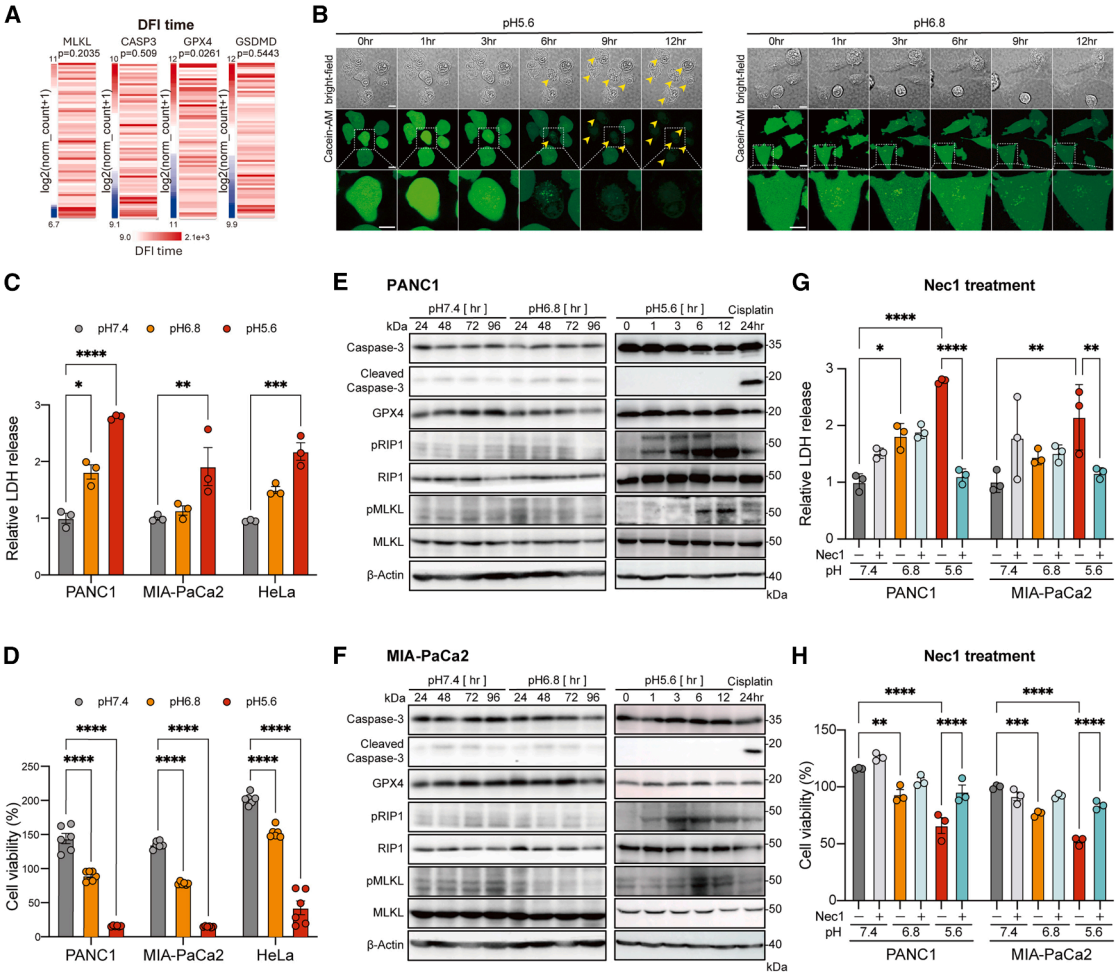

Figure 1. Necroptosis was induced in cancer cells under extreme acidity

(A) Heatmap illustrating disease-free survival (DFS) stratified by *MLKL*, *CASP3*, *GPX4*, and *GSDMD* expression levels (excluding null values from $n = 196$) in the Genomic Data Commons TCGA Pancreatic Cancer dataset. DFS probabilities were assessed using the log-rank test.

(B) Time-lapse images of calcein AM-stained MIA-PaCa2 cells exposed to different pH conditions. Stained cells indicate living cells, and arrowheads indicate sites of membrane rupture. Scale bars, 10 μm.

(C) Quantification of LDH release in three cell lines following 24-h incubation under varying pH conditions (pH 7.4, 6.8, and 5.6). Data are presented as means ± SEM ($n = 3$ biological replicates). Statistical analysis was performed by one-way analysis of variance (ANOVA). $^{*}p < 0.05$, $^{**}p < 0.01$, $^{***}p < 0.005$, $^{****}p < 0.001$.

(D) Cell viability of three cell lines cultured under different pH conditions (pH 7.4, 6.8, and 5.6), assessed by sulforhodamine B (SRB) staining. Data are presented as means ± SEM ($n = 3$ biological replicates). Statistical analysis was performed by one-way ANOVA. $^{****}p < 0.001$.

(E and F) Western blot analysis of key cell-death markers in PANC1 (E) and MIA-PaCa2 (F) cells cultured under different pH conditions. Protein levels of cleaved caspase-3, caspase-3, GPX4, phosphorylated RIP1 (pRIP1), RIP1, phosphorylated MLKL (pMLKL), and MLKL were analyzed over 24–96 h for pH 7.4 and 6.8 and over 0–12 h for pH 5.6. Cisplatin treatment for 24 h served as a positive control for apoptosis.

(G) LDH release assay in PANC1 and MIA-PaCa2 cells cultured under different pH conditions in the presence or absence of necrostatin-1 (Nec1), a necroptosis inhibitor. Cells were pretreated with vehicle or Nec1 for 1 h prior to exposure to acidic conditions. LDH release was measured after 6 h. Data are presented as means ± SEM ($n = 3$ biological replicates). Statistical analysis was performed by one-way ANOVA. $^{*}p < 0.05$, $^{**}p < 0.01$, $^{****}p < 0.001$.

(H) Cell viability of PANC1 and MIA-PaCa2 cells under different pH conditions in the presence or absence of Nec1 treatment. Cell viability was determined by SRB staining. Data are presented as means ± SEM ($n = 3$ biological replicates). Statistical analysis was performed by one-way ANOVA. $^{**}p < 0.01$, $^{***}p < 0.005$, $^{****}p < 0.001$.

Cancer cell adaptation to acidic conditions (pH 6.8)

While pH 6.8 did not induce typical programmed cell death, many floating pancreatic cancer cells were observed following exposures to pH 5.6 and pH 6.8. For PANC1 cells, 15.8% transitioned to a floating state at pH 6.8 and 45.3% at pH 5.6, whereas the remaining cells remained adherent (84.2% at pH 6.8 and 54.7% at pH 5.6) (Figures 2A and S3A). To examine whether floating cells at acidic pH survive or adhere, we developed a fractionation experiment in which floating cells from acidic conditions were collected and reintroduced to milder pH (pH 6.8, pH 6.8/pH 7.4, and pH 5.6 to pH 5.6/pH 6.8/pH 7.4) (Figure 2B). Both PANC1 and MIA-PaCa2 cells demonstrated recovery of adherence when transferred from pH 6.8 to pH 7.4 compared to those maintained under acidic conditions at pH 6.8 but not

Please cite this article in press as: Hasegawa et al., Tolerance to extracellular acidic pH facilitates tumor plasticity, Cell Reports (2026), https://doi.org/10.1016/j.celrep.2026.117226

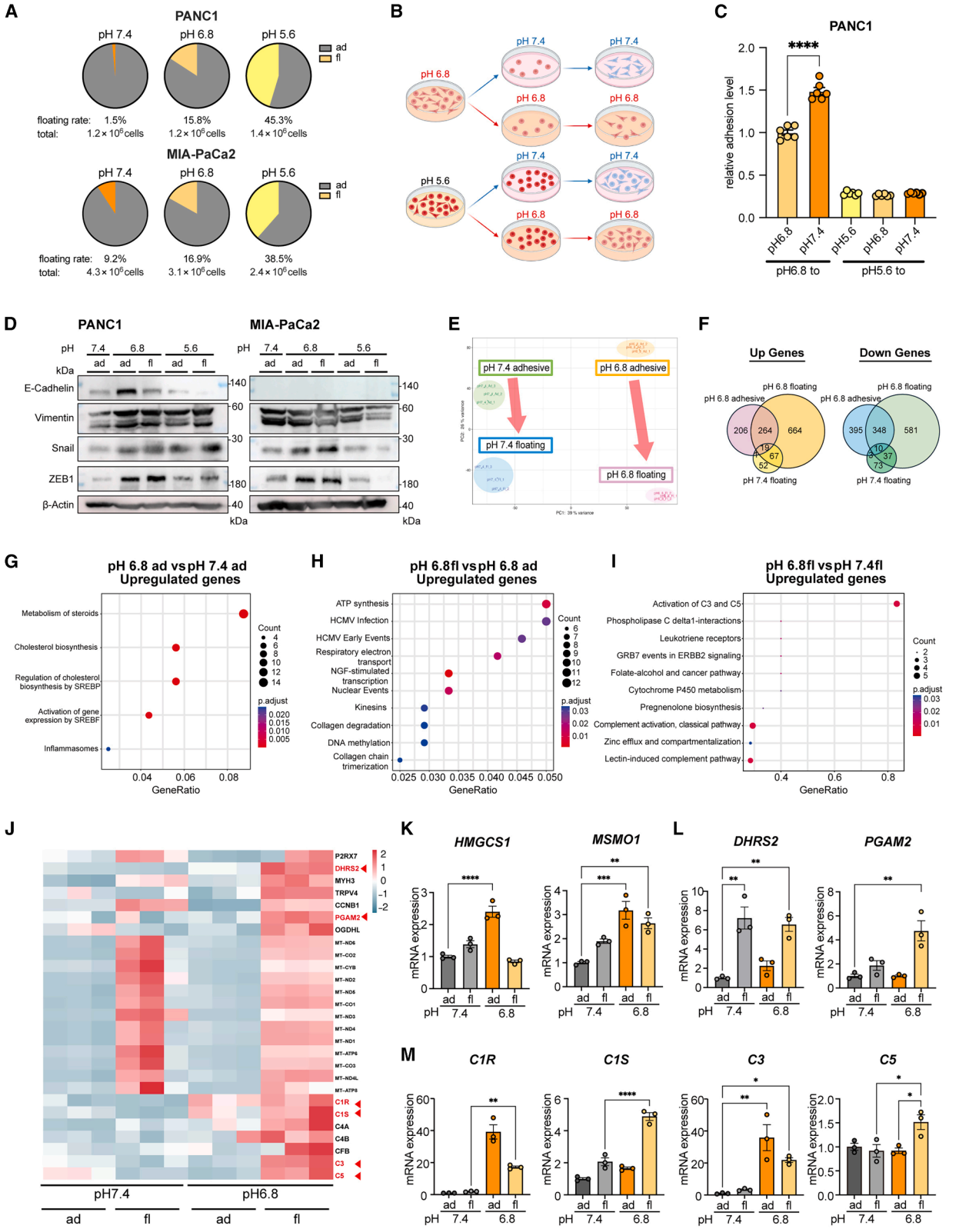

(legend on next page)

Please cite this article in press as: Hasegawa et al., Tolerance to extracellular acidic pH facilitates tumor plasticity, Cell Reports (2026), https://doi.org/10.1016/j.celrep.2026.117226

when transferred from pH 5.6 to pH 6.8 or 7.4 (Figures 2C and S3B), suggesting that acidic pH 6.8 induces EMT. Indeed, this adhesive transition correlated with increased expression of the EMT-related transcription factors, SNAIL and ZEB1, especially at pH 6.8 (Figure 2D).

Comprehensive RNA-sequencing (RNA-seq) analysis of adherent and floating PANC1 cells cultured at pH 7.4 or pH 6.8 for 24 h revealed distinct transcriptional profiles (Figure 2E), including 664 upregulated and 581 downregulated genes that were specific to floating cells at pH 6.8 (Figure 2F). Pathway analysis demonstrated activation of cholesterol biosynthesis pathways in adherent cells at pH 6.8 compared to those at pH 7.4 (Figure 2G). Meanwhile, extracellular matrix organization pathways were downregulated in floating cells at pH 6.8 compared to pH 6.8 adherent cells (Figure S3C). Both floating cells under pH 7.4 and pH 6.8, compared to adhesive cells under pH 7.4 and pH 6.8, enhanced ATP synthesis and respiratory electron transport (Figures 2H and S3D), while the cell-cycle regulation pathway was suppressed in pH 7.4 floating cells (Figures S3E and S3F). Moreover, a complement pathway was activated, including upregulation of *C3* and *C5* in pH 6.8 floating cells compared to floating cells at pH 7.4 (Figure 2I).

Specifically, the mRNA expression of cholesterol biosynthetic genes, such as *HMGCS1* and *MSMO1*, was upregulated in adhesive cells at pH 6.8 (Figure 2K), agreeing with previous studies.[24,25] In addition, metabolic genes involved in respiratory electron transport, such as *DHRS2* and *PGAM2*, were upregulated in pH 6.8 floating pancreatic cancer cells (Figure 2L). Upstream transcription factor analysis also indicated amplification of nuclear factor κB (NF-κB) signaling in floating cells at pH 6.8 (Figure S3G). mRNA expression of C1R, C1S, C3, and C5 was elevated in floating cells at pH 6.8 (Figures 2J and 2M). Other complement-pathway-related genes, including F2RL2 and SERPINA1, were also upregulated (Figures S4A and S4B), whereas CD59 and SERPINE1 expression was reduced (Figure S4B). Consistent with these transcriptional changes, C3 and C5 protein levels increased in PANC1 floating cells at pH 6.8 (Figure S4C) along with enhanced production of the activated fragments C3a and C5a (Figure S4D). Notably, genes within pathways activated under acute acidic conditions (Figures 2G–2I) remained similarly elevated or were further upregulated under chronic acidic pH conditions (Figures 3A, 3B, and S5A).

These results suggest that metabolic reprogramming involving the respiratory chain complex, and activation of the complement pathway may contribute to the survival of floating cells under acidic conditions (pH 6.8).

Tumorigenicity was preserved in floating cells under pH 6.8 conditions

To further investigate whether floating cells had tumorigenicity at pH 6.8, floating PANC1 and MIA-PaCa2 cells (pH 7.4 and pH 6.8) were subcutaneously injected into SCID/SCID mice, and tumor initiation was observed only in xenograft mice with pH 6.8 floating cells (7 out of 8 mice in pH 6.8 floating vs. 0 out of 8 mice in pH 7.4 floating) (Figures 3C and 3D). These findings suggest that the pH 6.8 floating cells maintained their viability and tumorigenicity. Furthermore, tumor size was measured over a 21-day period. Tumor formation was observed in floating cells at pH 6.8; in comparison, a limited tumor-forming ability was observed in cells at pH 7.4 (Figures 3E and S5B). Immune-cell infiltration within the tumors was assessed by immunostaining (Figure 3F). The analysis revealed an increase in CD11b-positive cells (monocytes, natural killer [NK] cells, granulocytes, and macrophages), F4/80-positive cells (macrophages), Ly6G-positive cells (neutrophils), and CD31-positive blood vessel cells in tumors derived from pH 6.8 floating cells in the MIA-PaCa2 xenograft model (Figure 3G). The surviving floating cells at pH 6.8 demonstrated immunomodulation, potentially through the activation of the complement pathway. In summary, at pH 7.4, most cells remained adherent and viable, while floating cells were largely non-viable. In contrast, floating cells at pH 6.8 remained viable and retained tumorigenic potential. At pH 5.6, most cells detached and underwent necroptosis (Figure 3H).

Figure 2. Cancer cell adaptation to acidic conditions (pH 6.8)

(A) Proportion of floating cells in PANC1 and MIA-PaCa2 cultures under different pH conditions. Cells were counted after medium replacement for 24 h to determine the number of adherent (ad) and floating (fl) cells. The percentage of floating cells and the total cell numbers are shown below each pie chart.

(B) Schematic of the experimental design for the adhesion recovery assay. Floating cells derived from acidic conditions were collected and reintroduced into the same or different pH environments (pH 6.8 to pH 6.8/pH 7.4; pH 5.6 to pH 5.6/pH 6.8/pH 7.4). Cells were cultured for 48 h, and proliferation was assessed by SRB assay.

(C) Quantification of adhesion recovery in PANC1 cells based on proliferation assays. Data are presented as means ± SEM of $n = 6$ biological replicates. Statistical analysis was performed by one-way ANOVA. $^{****}p < 0.001$.

(D) Western blot analysis of EMT markers in PANC1 and MIA-PaCa2 cells. Protein expression was evaluated after 24 h of culture at pH 5.6, pH 6.8, and pH 7.4. Adherent (ad) and floating (fl) cell populations were separated prior to analysis.

(E) Principal-component analysis of RNA-seq showing distinct transcriptomic patterns between cellular floating and adhesive states at pH 6.8 and pH 7.4.

(F) Venn diagram showing genes upregulated (left) and downregulated (right) in cells exposed to different conditions for 24 h, compared with adherent cells at pH 7.4.

(G–I) Gene Ontology (GO) enrichment analysis of molecular function terms for upregulated differentially expressed genes (DEGs) between pH 6.8 adhesion (ad) and pH 7.4 adhesion (G), pH 6.8 adhesion and floating (fl) (H), and pH 6.8 floating and pH 7.4 floating (I). Dotplots display GO terms enriched among upregulated DEGs. Dot color represents the *p* value, and dot size indicates the count of DEGs associated with each GO term.

(J) Heatmap of transcript abundance in enriched genes from 20 respiratory systems and seven complement pathways in floating (fl) and adherent (ad) cells of pH 6.8 and pH 7.4. Genes labeled in red were validated by RT-qPCR.

(K–M) mRNA expression levels of the cholesterol biosynthetic pathway (K), metabolic enzymes (L), and the complement pathway (M) in PANC1 adherent (ad) and floating (fl) cells under pH 7.4 and pH 6.8. Data are presented as means ± SEM of $n = 3$ biological replicates. Statistical analysis was performed by one-way ANOVA. $^{*}p < 0.05$, $^{**}p < 0.01$, $^{***}p < 0.005$, $^{****}p < 0.001$.

Please cite this article in press as: Hasegawa et al., Tolerance to extracellular acidic pH facilitates tumor plasticity, Cell Reports (2026), https://doi.org/10.1016/j.celrep.2026.117226

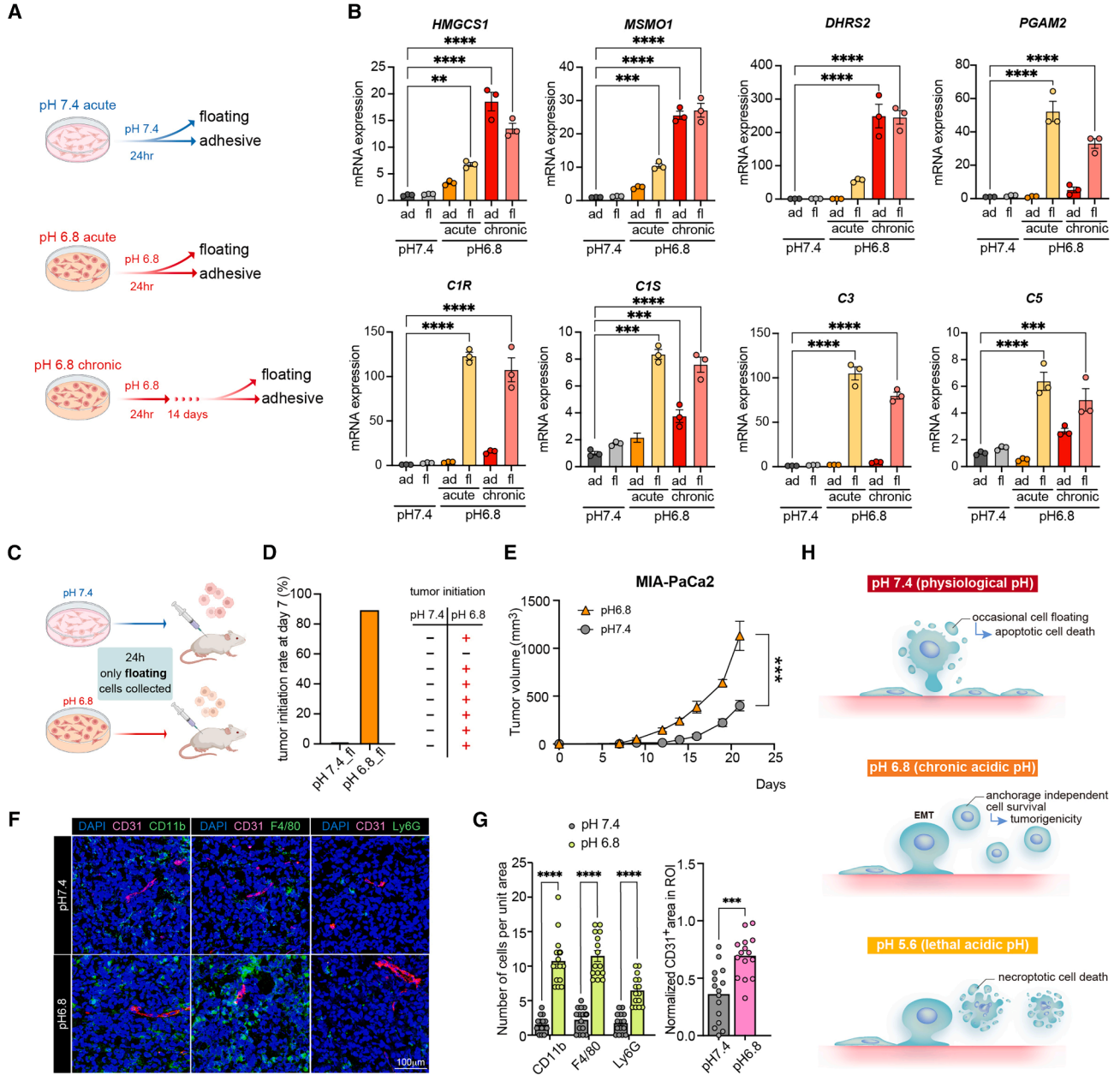

Figure 3. Floating cells under pH 6.8 retain tumorigenic potential

(A) Schematic of acute and chronic culture of PANC1 cells under normal (pH 7.4) and acidic (pH 6.8) conditions. For acute exposure, cells were cultured for 24 h at pH 7.4 or pH 6.8. For chronic exposure, cells were cultured at pH 6.8 for 14 days, with intermittent recovery at pH 7.4 to maintain cell numbers. After each condition, adherent and floating cells were separated and collected.

(B) mRNA expression of genes involved in cholesterol biosynthesis (HMGCS1 and MSMO1), cellular energy metabolism (DHRS2 and PGAM2), and the complement pathway (C1R, C1S, C3, and C5) in adherent (ad) and floating (fl) PANC1 cells cultured at pH 7.4 or pH 6.8 under acute and chronic exposure. $n = 3$ biological replicates. Data are presented as means ± SEM. Statistical analysis was performed by unpaired two-tailed Student's t test. $^{**}p < 0.01$, $^{***}p < 0.005$, $^{****}p < 0.001$.

(C) Schematic of the subcutaneous tumor model using floating MIA-PaCa2 cells cultured at pH 7.4 or pH 6.8. Floating cells were isolated from each condition and injected subcutaneously at 5×10^6 cells in 100 μL of PBS ($n = 8$ per group).

(D) Tumor formation ratio at 7 days post injection for floating cells cultured at pH 7.4 or pH 6.8 ($n = 8$ per group).

(E) Tumor growth curves for mice injected with floating cells cultured at pH 7.4 or pH 6.8 ($n = 8$ per group). Data are presented as means ± SEM. Statistical analysis was performed by unpaired two-tailed Student's t test. $^{***}p < 0.005$.

(legend continued on next page)

Please cite this article in press as: Hasegawa et al., Tolerance to extracellular acidic pH facilitates tumor plasticity, Cell Reports (2026), https://doi.org/10.1016/j.celrep.2026.117226

FAM129C functions as a pH-dependent tumor suppressor

Acidic pH stimulates anchorage-independent cell survival, plasticity, and tumor initiation. To identify regulators of chronic acid tolerance, we established a chronic acidic culture system by reducing the bicarbonate concentration in the culture medium to maintain an pHe of 6.8 at 37°C under 5% CO_2 conditions. To maintain cell viability during long-term culture, cells were incubated at pH 6.8 for 24 h, followed by recovery culture at pH 7.4 for 48 h. We then conducted genome-wide CRISPR knockout screening using the Toronto Knockout CRISPR Library version 3, which was introduced into pancreatic cancer cells, PANC1, using a lentiviral system[30] (Figure 4A). The enrichment rate of the guide RNAs (gRNAs) was determined using MAGeCK.[31] The counts of each gRNA were obtained from fastq files in count mode, and significantly altered gRNAs were extracted in the comparison mode (Figure 4A).

The variation in the counts was calculated as the robust rank aggregation score for each gene. The top gRNA-targeted genes that significantly increased under acidic pH conditions included *MED12*, *TADA1*, *PBX4*, *MYO1A*, *PDGFRA*, *FAM129C*, and *TADA2B* (Figure 4B). The top ten gRNA-targeted genes associated with acidic pH screening were significantly correlated with poor prognosis in patients with PAAD (Figure 4C) and various other cancer types (Figure S6A). To identify which of these top ten genes contributed most to patient prognosis, prognostic analysis was performed on the genes identified by gRNA screening based on gene-expression changes in clinical specimens from patients with pancreatic cancer in The Cancer Genome Atlas (TCGA) (Figures 4D and S6C). *FAM129C* was identified as the top contributing gene associated with improved patient survival in PAAD and lung adenocarcinoma (Figures 4D, S6B, and S6C).

To investigate the potential contribution of *FAM129C* to cell survival under acidic pH of 6.8, we generated stable FAM129C knockout PANC1 cells (Figure 4E). We cultured *FAM129C* knockout cells at pH 6.8 for 72 h and performed proliferation assays. *FAM129C* knockout cells exhibited significantly enhanced proliferation compared to the control cell line at pH 7.4 and particularly at pH 6.8, indicating the essential role of *FAM129C* in cell survival under prolonged acidic pH stress (Figure 4F). To further investigate the function of *FAM129C* in cancer cells, we generated stable FAM129C-overexpressing PANC1 and MIA-PaCa2 cells by lentiviral infection using the pMX-FAM129C vector and confirmed their protein levels (Figures 4G and S6D). No significant differences in proliferation were observed in FAM129C-overexpressing PANC1 or MIA-PaCa2 cells compared to control cells (Figure 4H). To examine the role of FAM129C in mouse pancreatic tumors, we generated murine pancreatic cancer (Pan02) cells overexpressing FAM129C, subcutaneously transplanted them into immunocompetent C57BL/6NJcl mice, and monitored tumor growth over time. FAM129C overexpression significantly suppressed tumor growth in syngeneic Pan02 tumors (Figure 4J). Significant tumor suppression due to FAM129C overexpression was observed in xenografts of both PANC1 and MIA-PaCa2 cells (Figures 4K and S6F), indicating that FAM129C acts as a tumor suppressor at an acidic pH. Furthermore, FAM129C knockout resulted in reduced expression of phosphorylated RIP1 (pRIP1) and phosphorylated MLKL (pMLKL), suggesting that FAM129C potentially played a role in regulating necroptosis avoidance at pH 5.6 (Figure S6E).

FAM129C regulates tumor immunity through PIGR

FAM129C expression was negatively correlated with the expression of acidic pH-responsive *HMGCS1* and *MSMO1* genes in TCGA pancreatic cancer patients, both of which are upregulated at pH 6.8 (Figure S7A). Given that FAM129C overexpression did not inhibit cell growth *in vitro* but significantly suppressed tumor growth *in vivo*, we employed a PANC1 xenograft mouse model to further investigate this phenomenon and downstream targets of FAM129C. To explore the key regulator of immunomodulation, the transplanted tumor was excised approximately 20 days after transplantation, and the extracted RNA was subjected to RNA-seq. Compared to the control group, genes with altered expression in FAM129C-overexpressing groups are represented in a volcano plot based on *p* values and fold-change ratios (Figure 5A). Overexpression of *FAM129C* was confirmed within tumor tissues, and altered expression of genes such as *PNMA2*, *DLG1*, *LAMB3*, and *PIGR* was observed (Figure 5A). Genes that were significantly up-/downregulated (2-fold) were subjected to pathway analysis.[32] In FAM129C-overexpressing tumor tissues, downregulation of cytokine-related pathways was observed owing to decreased expression (Figure 5B). Additionally, a significant reduction in the mRNA expression of *PIGR*, as well as *CCL5*, *CCL16*, *IL10*, and *IL10RA*, was observed (Figure 5C) along with downregulation of the IL-6 signaling pathway (Figure S7B) and NF-κB1 expression (Figure S7C). These transcriptional changes in immunosuppressive remodeling may demonstrate similarity to those observed in tumors derived from surviving floating cells at pH 6.8, where inflammatory gene expression was also upregulated.

PIGR has been identified as a potential regulator of tumor immunity.[33] Therefore, we focused on the role of PIGR in tumor immunity. To analyze the role of PIGR in mouse tumor tissues, cells stably overexpressing PIGR were established by transfecting PANC1 cells with the pMX-PIGR vector via viral infection (Figure 5D). PIGR-overexpressing PANC1 cells were subcutaneously transplanted into CB17/IcrJcl-Prkdcscid mice, and the tumor volume was measured. A significant increase in tumor

(F) Immunostaining of tumors excised from mice bearing MIA PaCa-2 xenografts derived from floating cells cultured at pH 7.4 or pH 6.8. Vascular endothelial cells were labeled with CD31, myeloid cells with CD11b, macrophages with F4/80, and neutrophils with Ly6G. Nuclei were counterstained with DAPI. Scale bar, 100 μm.

(G) Quantification of $CD11b^+$, $F4/80^+$, and $Ly6G^+$ cells (left) and $CD31^+$ area (right) shown in (F). Data are presented as means ± SEM. Statistical analysis was performed by unpaired two-tailed Student's *t* test. $^{***}p < 0.005$, $^{****}p < 0.001$.

(H) Model of cellular responses under different pH conditions. At pH 7.4 (left), most cells remained adherent, whereas floating cells underwent apoptosis. At pH 6.8 (middle), a subset of cells persisted in a floating state, continued to proliferate, and retained tumorigenic potential. At pH 5.6 (right), most cells detached and underwent necroptosis.

Please cite this article in press as: Hasegawa et al., Tolerance to extracellular acidic pH facilitates tumor plasticity, Cell Reports (2026), https://doi.org/10.1016/j.celrep.2026.117226

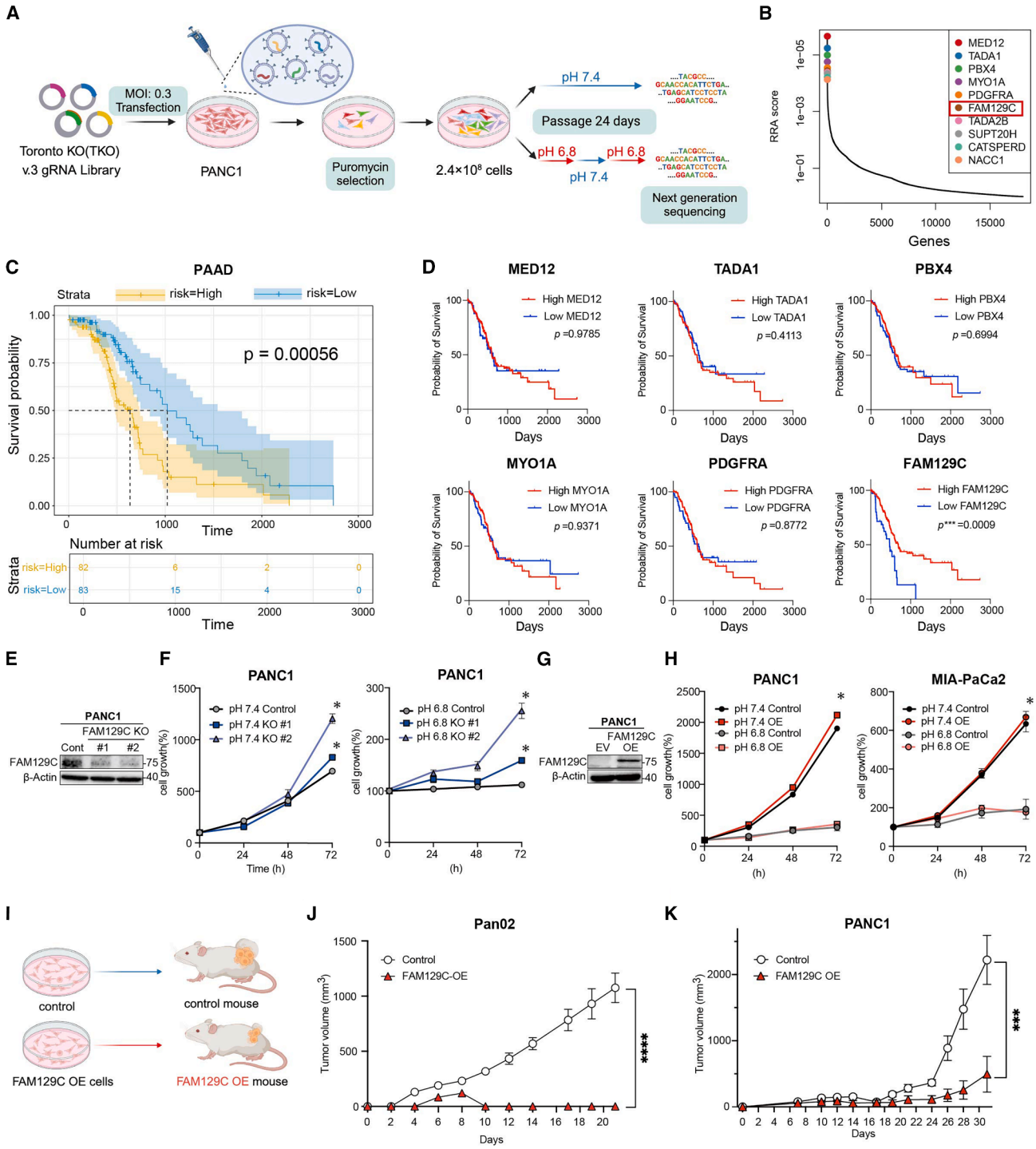

Figure 4. FAM129C functions as a pH-dependent tumor suppressor

(A) Experimental schematic of CRISPR knockout screening in PANC1 cells cultured under normal (pH 7.4) and acidic (pH 6.8) conditions, followed by gRNA-sequencing analysis. To maintain cell viability under pH 6.8 treatment, cells were cultured at pH 6.8 for 24 h, then switched to pH 7.4 for 48 h, and subsequently returned to pH 6.8.

(B) gRNA screening results showing a robust rank aggregation (RRA) score of 18,053 genes calculated by MAGeCK-VISPR. Lower RRA scores indicate greater essentiality under acidic conditions. The top ten enriched genes under pH 6.8 are highlighted.

(legend continued on next page)

Please cite this article in press as: Hasegawa et al., Tolerance to extracellular acidic pH facilitates tumor plasticity, Cell Reports (2026), https://doi.org/10.1016/j.celrep.2026.117226

growth due to PIGR overexpression was observed in PANC1 xenografts (Figure 5E). Immunohistochemical staining of immune-cell markers was performed on frozen sections. The analysis revealed an increase in CD11b-positive cells, F4/80-positive cells, Ly6G-positive cells, and CD31-positive blood vessel cells in PIGR-overexpressing tumor tissues in PANC1 xenograft tumor (Figures 5F and 5G). We next investigated immunocompetent mice (C57BL/6JJclC57BL/6NJcl). To further investigate whether overexpression of PIGR regulates immune modulation within tumors, PIGR-overexpressing Pan02 cells were generated and subcutaneously inoculated into C57/BL6 immune-proficient mice (Figure 5H). PIGR-overexpressing Pan02 cells exhibited increased tumor growth (Figure 5I) and enhanced immune-cell recruitment, consistent with our observations in PANC1 and HSML cells (Figures 5E and S8A–S8D). Immune profiling further showed that PIGR overexpression increased macrophage ($CD45^+F4/80^+CD11b^+$) infiltration while reducing infiltration of monocytes ($CD45^+F4/80^-Ly6C^{high}Ly6G^-$), dendritic cells, $CD8^+$ T cells, and B cells within tumors (Figures 5J–5M). However, no significant changes were observed in exhaustion-associated or stemness-associated (stem-like) T cell phenotypes, nor in macrophage polarization, upon PIGR overexpression (Figures S8F–S8H). This suggests that the inhibition of the infiltration of macrophages through complement inhibitors may reduce PIGR-overexpressing tumors.

Anti-PD-L1 and complement inhibition synergistically suppressed PIGR-overexpressing tumors

Increased PIGR expression through FAM129C loss is one of the key factors for acidic pH adaptation and tumor progression. Given that the complement pathway was strongly activated in floating cells at pH 6.8 for increased macrophage infiltration and that PIGR-overexpressing tumors also exhibited increased macrophage infiltration, we hypothesized that targeting the combination of the complement and immune checkpoint systems might enhance therapeutic outcomes. Therefore, we administered PMX-53, a synthetic cyclic peptide antagonist of the C5a receptor (C5aR1/CD88), combined with the anti-programmed cell-death ligand 1 (PD-L1) antibody. This combination treatment exerted a synergistic anti-tumor effect in PIGR-overexpressing Pan02 and HMSL tumors, suggesting that dual blockade of PD-L1 and complement signaling (C5aR1) may represent a therapeutic strategy for tumors adapted to acidic environments (Figures 6A, 6B, S9A, and S9B).

To examine the infiltration of immune cells following PD-L1 and complement signaling (C5aR1) blockade, we performed immune staining of the tumor tissues (Figure 6C). The frequency of $CD8^+$ T cells was higher in the control group compared to all PIGR-overexpressing groups. Notably, the proportion of interferon-γ (IFN-γ)$^+CD8^+$ T cells was significantly elevated in the PIGR-overexpressing combination group relative to the other groups (Figures 6C, 6D, S6C, and S6D). Additionally, infiltration of $F4/80^+$ macrophage was significantly suppressed in the PIGR-overexpressing combination group (Figures 6C, 6D, S6C, and S6D).

These results indicate that in PIGR-overexpressing tumors, the combination of PD-L1 blockade and inhibition of the complement pathway—activated in floating cells at pH 6.8—elicits a pronounced synergistic anti-tumor effect (Figure 6E).

DISCUSSION

Acidic extracellular pH is a hallmark of the tumor microenvironment, yet cellular responses to severe acidosis are highly context dependent. Several cell-death pathways have been reported under acidic conditions, including caspase-dependent apoptosis in chondrocytes,[21] ferroptosis in breast cancer,[22] and pyroptosis in liver injury.[23] In contrast, our study identifies necroptosis as the predominant cell-death pathway induced by acidic pH in pancreatic cancer cells. The ability of Nec1 to prevent cell death by disrupting RIP1-RIP3-MLKL signaling supports a mechanistic role for necroptosis and suggests potential therapeutic relevance. This is particularly notable given accumulating evidence that pharmacological induction of necroptosis can exert anti-tumor activity in multiple cancer types, including pancreatic cancer and triple-negative breast cancer.[34,35] Notably, necroptosis appears to be suppressed under moderately acidic conditions (pH 6.8) representing a commonly observed pH in solid tumors, indicating that pancreatic cancer cells may adopt alternative survival strategies under these conditions.

Consistent with this notion, a key finding of our study was the identification of survival mechanisms that enable pancreatic

(C) Overall survival (OS) of patients with pancreatic cancer, calculated using the TCGA PAAD dataset. Patients were stratified into high-risk (log risk > 0) and low-risk (log risk < 0) groups based on the Cox proportional hazards model, using the expression levels of the top ten upregulated gRNA genes under acidic pH conditions identified in CRISPR knockout screening (*MED12*, *TADA1*, *PBX4*, *MYO1A*, *PDGFRA*, *FAM129C*, *TADA2B*, *SUPT20H*, *CATSPERD*, and *NACC1*).
(D) Prognostic analysis of the top six gRNA-targeted genes in pancreatic cancer.
(E) Western blot analysis of FAM129C knockdown in PANC1 cells. Actin is shown as a loading control in the lower panel.
(F) Results of cell growth measurements in FAM129C knockdown PANC1 cells cultured under pH 7.4 (left) or pH 6.8 (right) conditions at 24, 48, and 72 h after seeding. Cell viability was quantified by SRB staining. Data are presented as means ± SEM ($n = 3$ biological replicates). Statistical analysis was performed by unpaired two-tailed *t* test. $^*p < 0.05$.
(G) Western blot analysis of FAM129C-overexpressing PANC1 cells (top) and MIA-PaCa2 cells (bottom). Actin is shown as a loading control.
(H) Results of cell growth measurements in control and FAM129C-overexpressing PANC1 (left) and MIA-PaCa2 cells (right) cultured under pH 7.4 or pH 6.8 conditions at 24, 48, and 72 h after seeding. Cell viability was quantified by SRB staining. Data are presented as means ± SEM ($n = 3$ biological replicates). Statistical analysis was performed by unpaired two-tailed *t* test. $^*p < 0.05$.
(I) Schematic of subcutaneous tumor models established using control or FAM129C-overexpressing PANC1 cells. 5×10^6 cells in 100 μL of PBS were subcutaneously injected into SCID mice. $n = 5$ per group.
(J and K) Tumor growth curves of control and FAM129C overexpressing Pan02 syngeneic ($n = 5$ biological replicates) (J) and PANC1 xenograft tumor models ($n = 5$ biological replicates) (K). Tumor cells (1×10^7 control or FAM129C knockout PANC1 or Pan02 cells suspended in 100 μL of PBS) were subcutaneously injected into SCID or C57BL/6J mice, respectively. Data are presented as means ± SEM. Statistical analysis was performed by Student's *t* test. $^{***}p < 0.005$, $^{****}p < 0.001$.

Please cite this article in press as: Hasegawa et al., Tolerance to extracellular acidic pH facilitates tumor plasticity, Cell Reports (2026), https://doi.org/10.1016/j.celrep.2026.117226

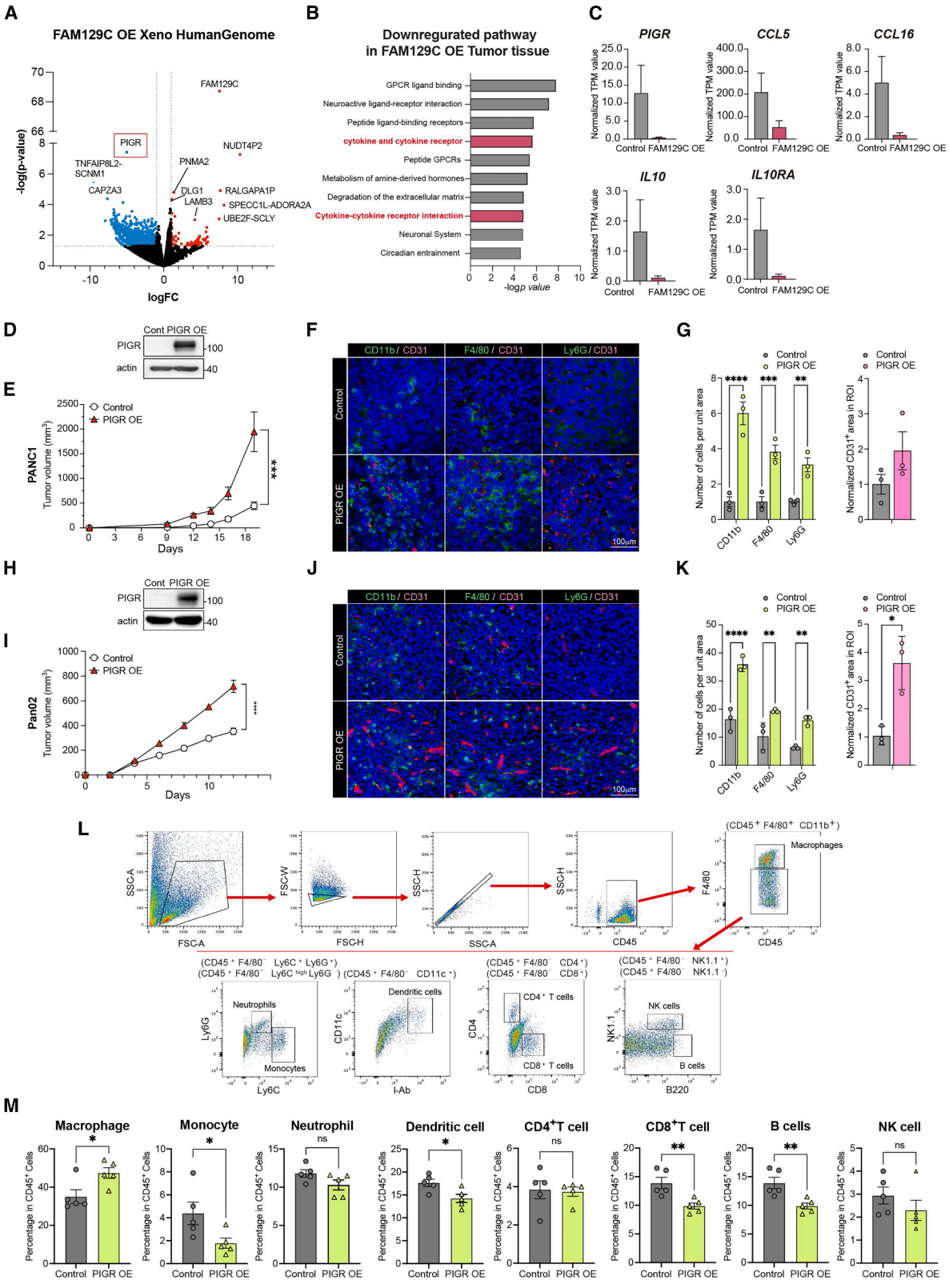

(legend on next page)

Please cite this article in press as: Hasegawa et al., Tolerance to extracellular acidic pH facilitates tumor plasticity, Cell Reports (2026), https://doi.org/10.1016/j.celrep.2026.117226

cancer cells to persist in an anchorage-independent state under moderate tumor acidosis (pH 6.8). However, our data challenge this assumption by showing that, at pH 6.8, a subset of PANC1 and MIA-PaCa2 cells remain viable despite loss of attachment and also acquire increased tumorigenicity. Survival in this floating state may be supported by upregulation of EMT-associated gene programs, consistent with an adaptive response to acidic stress. This extends prior reports of acid-induced EMT[36,37] by demonstrating that acidosis induces a reversible, survival-promoting state that preserves proliferative capacity even in floating cells.

Previous studies have highlighted the importance of OXPHOS[9] and have reported differential expression of cholesterol biosynthetic genes in adherent cells.[24] However, in contrast to adherent cells, we found that floating cancer cells exhibit a distinct transcriptional program, including enrichment of complement-related pathways (e.g., activation of C3 and C5), which we consider an additional finding of this study. Notably, transplantation of these cells into SCID/SCID mice resulted in robust tumor formation accompanied by increased immune-cell infiltration. Consistently, activation of the classical complement cascade has been shown to promote tumor-associated macrophage recruitment and establish an immunosuppressive niche.[38] Together, these findings suggest that anchorage-independent cancer cells adapted to pH 6.8 may actively shape the immune microenvironment through complement signaling.

Through genome-wide CRISPR screening, we identified *FAM129C* as a critical regulator of acid tolerance under long-term acidic pH of 6.8. FAM129C was originally characterized as a B-cell-specific plasma membrane protein (BCNP1) containing a pleckstrin homology domain, proline-rich motifs, and an SH2 binding motif.[39] Our findings extend the understanding of FAM129C function in tumor suppression under acidic conditions by the significant suppression of tumor growth observed in xenograft experiments with FAM129C-overexpressing PANC1 cells. FAM129C may also contribute to the evasion of necroptosis, highlighting its potential role in acidic-pH-induced cell death under acidic tumor microenvironments.

Transcriptome analysis of these tumors revealed regulatory networks involving *PIGR*, *PNMA2*, *DLG1*, and *LAMB3*, with PIGR being particularly notable as it exhibits context-dependent functions in pancreatic cancer. In pancreatic cancer cells exposed to pancreatic stellate cells, PIGR upregulation promotes poor patient prognosis,[40] whereas its downregulation occurs through cytokine-dependent mechanisms within the tumor microenvironment,[41,42] which is consistent with our observed reduction in tumor-promoting cytokines in FAM129C-overexpressing tissues between FAM129C and PIGR. Furthermore, our findings suggest that within the FAM129C tumor, PIGR mediates complement signaling and macrophage infiltration. Consistent with this notion, tumors overexpressing PIGR exhibited increased macrophage infiltration accompanied by reduced infiltration of $CD8^+$ T cells as well as decreased infiltration of monocytes, dendritic cells, and B cells (Figure 5M). Our analyses showed no significant changes in the proportions of exhaustion-associated or stemness-associated $CD8^+$ T cell subsets. These observations indicate that PIGR-dependent macrophage regulation may influence the immune landscape without markedly altering the phenotypic states of anti-tumor $CD8^+$ T cells. Further detailed studies will be required to more carefully assess whether, and to what extent, PIGR-dependent macrophage modulation influences $CD8^+$ T cell function and differentiation within the tumor.

We found that the dual targeting of PD-L1 and the complement pathway has a synergistic anti-tumor effect on the overexpression of PIGR, a downstream effector of pH 6.8

Figure 5. FAM129C regulates tumor immunity through PIGRs

(A) Volcano plot showing DEGs in FAM129C-overexpressing tumor tissues. Upregulated genes ($\log_2$ fold change > -1, $p < 0.05$) are shown in red, downregulated genes ($\log_2$ fold change < -1, $p < 0.05$) in blue, and non-significant genes ($|\log_2$ fold change$| \leq 1$, $p \geq 0.05$) in black.

(B) Pathway enrichment analysis of downregulated genes ($\log_2$ fold change < -1, $p < 0.05$) in FAM129C-overexpressing tumor tissues.

(C) Transcripts per million (TPM) values of *PIGR* and cytokine-related gene-expression levels within control and FAM129C-overexpressing tumor tissues. Data are presented as means ± SEM of $n = 3$ biological replicates. Statistical analysis was performed by unpaired two-tailed Student's *t* test.

(D) Western blot analysis confirming the establishment of PIGR-overexpressing (OE) PANC1 cells.

(E) Tumor growth curves of control and PIGR-OE PANC1 xenografts. 5×10^6 cells in 100 μL of PBS were subcutaneously injected into SCID mice. $n = 5$ per group. Data are presented as means ± SEM of $n = 5$ biological replicates. Statistical analysis was performed by unpaired two-tailed Student's *t* test. $^{***}p < 0.005$.

(F) Immunofluorescence staining of PANC1 tumors derived from control and PIGR-OE PANC1 xenografts described in (E). Markers are shown as follows: CD31 (endothelial cells), CD11b (myeloid cells), F4/80 (macrophages), and Ly6G (neutrophils). Nuclei were counterstained with DAPI. Scale bar, 100 μm.

(G) Quantification of cell number of $CD11b^+$ cells, $F4/80^+$ cells, and $Ly6G^+$ cells (left) and $CD31^+$ area (right) in (F). Data are presented as means ± SEM of $n = 3$ biological replicates. Statistical analysis was performed by unpaired two-tailed Student's *t* test. $^{**}p < 0.01$, $^{***}p < 0.005$; $^{****}p < 0.001$.

(H) Western blot analysis confirming the establishment of PIGR-OE Pan02 cells.

(I) Tumor growth curves of syngeneic control and PIGR-OE Pan02 tumors. Tumor cells (1×10^7 control or PIGR-OE Pan02 cells suspended in 100 μL of PBS) were subcutaneously injected into C57BL/6J mice. Data are presented as means ± SEM of $n = 8$ biological replicates. Statistical analysis was performed by unpaired two-tailed Student's *t* test. $^{***}p < 0.005$.

(J) Immunofluorescence staining of syngeneic Pan02 tumors collected from mice described in (I). Vascular endothelial cells were labeled with CD31, myeloid cells with CD11b, macrophages with F4/80, and neutrophils with Ly6G. Nuclei were counterstained with DAPI. Scale bar, 100 μm.

(K) Quantification of cell number of $CD11b^+$ cells, $F4/80^+$ cells, and $Ly6G^+$ cells (left) and $CD31^+$ area (right) in (J). Data are presented as means ± SEM of $n = 3$ biological replicates. Statistical analysis was performed by unpaired two-tailed Student's *t* test. $^{*}p < 0.05$, $^{**}p < 0.01$, $^{****}p < 0.001$.

(L) Schematic of the experimental workflow and gating strategy for fluorescence-activated cell sorting (FACS) of $CD45^+$ immune cells isolated from syngeneic Pan02 tumors. $CD45^+$ cells were further gated to identify monocytes ($CD45^+F4/80^-Ly6C^{high}Ly6G^-$), tumor-associated macrophages ($CD45^+F4/80^+CD11b^+$), neutrophils ($CD45^+F4/80^-Ly6C^+Ly6G^+$), dendritic cells ($CD45^+F4/80^-CD11c^+I\text{-}Ab^+$), $CD4^+$ T cells ($CD45^+F4/80^-CD4^+$), $CD8^+$ T cells ($CD45^+F4/80^-CD8^+$), NK cells ($CD45^+F4/80^-NK1.1^+$), and B cells ($CD45^+F4/80^-B220^+$). Representative gating plots are shown for control and PIGR-OE syngeneic Pan02 tumors.

(M) Quantification of the proportions of $CD45^+$ immune-cell subsets in control and PIGR-OE syngeneic Pan02 tumors. Data are presented as means ± SEM of $n = 3$ biological replicates. Statistical analysis was performed by unpaired two-tailed Student's *t* test. $^{*}p < 0.05$, $^{**}p < 0.01$; ns, not significant.

Please cite this article in press as: Hasegawa et al., Tolerance to extracellular acidic pH facilitates tumor plasticity, Cell Reports (2026), https://doi.org/10.1016/j.celrep.2026.117226

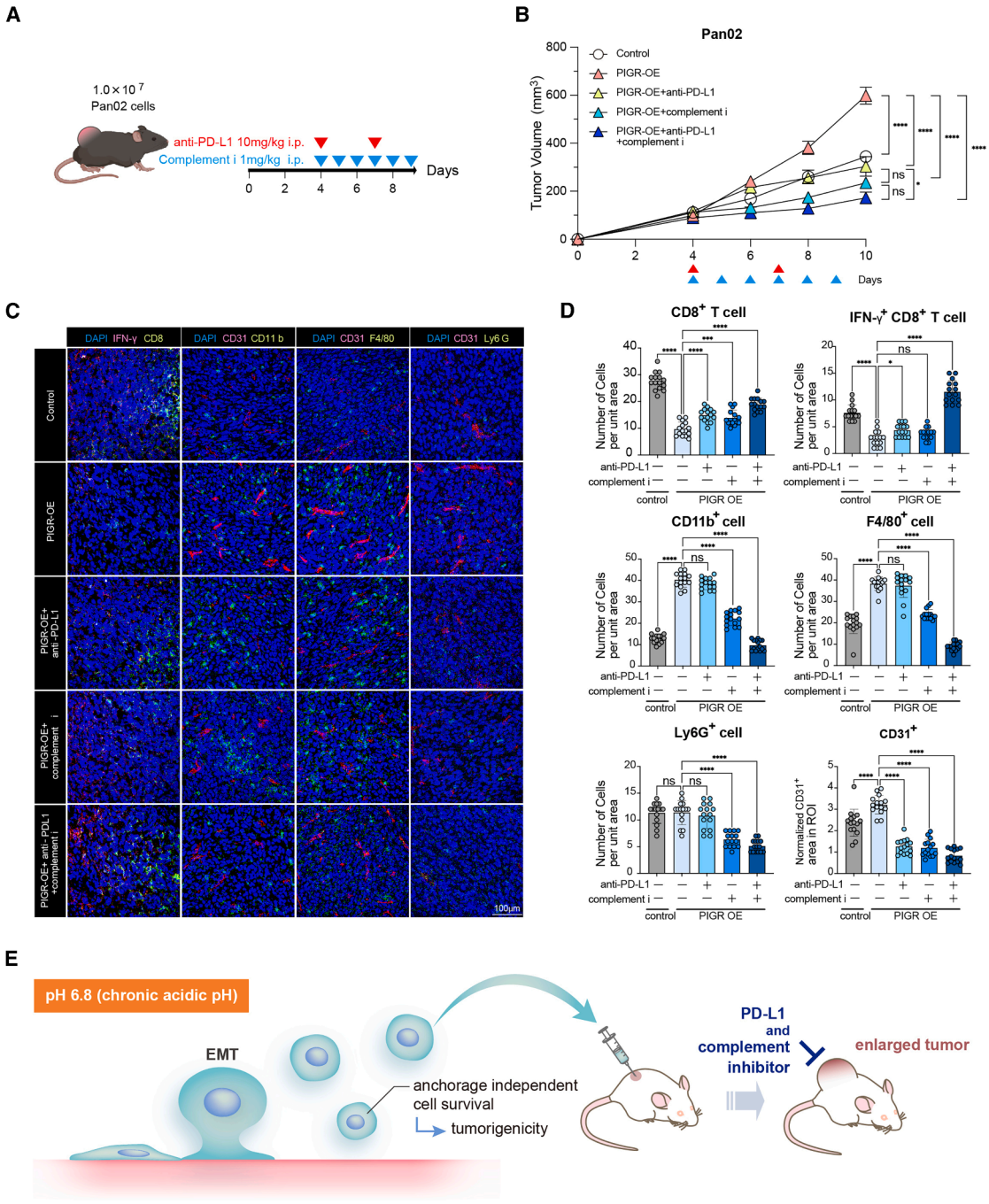

Figure 6. Anti-PD-L1 and complement inhibition synergistically suppressed PIGR-overexpressing tumors

(A) *In vivo* experiment scheme. Tumor cells (1×10^7 control or PIGR-overexpressing Pan02 cells suspended in 100 μL of PBS) were subcutaneously injected into C57BL/6J mice. The control group received PBS from day 4, while PIGR-overexpressing (PIGR-OE) groups were treated with either PBS daily from day 4, anti-PD-L1 antibody on days 4 and 7, PMX53 (a complement inhibitor) every day from day 4, or a combination of anti-PD-L1 antibody and PMX53 intraperitoneally.

(B) Tumor growth curves of syngeneic Pan02 tumors described in (A). Tumor growth was monitored every 2 days ($n = 5$ mice per group). Tumor samples were collected for further analyses on day 10. Data are presented as means ± SEM of $n = 5$ biological replicates. Statistical analysis was performed by two-way ANOVA. $^*p < 0.05$, $^{****}p < 0.001$; ns, not significant.

(C) Immunofluorescence staining of syngeneic Pan02 tumors collected from mice described in (A). The indicated markers are shown as follows: CD31 (vascular endothelial cells), CD11b (myeloid cells), F4/80 (macrophages), Ly6G (neutrophils), CD8 (cytotoxic T cells), and IFN-γ (IFN-γ-producing cells). Nuclei were counterstained with DAPI. Scale bar, 100 μm.

(legend continued on next page)

Please cite this article in press as: Hasegawa et al., Tolerance to extracellular acidic pH facilitates tumor plasticity, Cell Reports (2026), https://doi.org/10.1016/j.celrep.2026.117226

adaptation. PIGR has been shown to mediate the uptake of immunoglobulin A dimers and promote macrophage infiltration,[43] which is supported by our data. Given that with the infiltration of tumor-associated macrophages (TAMs), anti-PD-L1 can bind to the surface of TAMs—thereby limiting its availability to effector T cells[44]—we propose that complement inhibition reduces macrophage infiltration,[45] thus enhancing the delivery of anti-PD-L1 to $CD8^+$ T cells and improving therapeutic efficacy.

In conclusion, this study identified necroptosis as the predominant cell-death mechanism under extremely acidic conditions (pH 5.6) and highlighted the role of FAM129C- and PIGR-mediated regulation of tumor immunity in facilitating cancer cell survival at moderate acidity (pH 6.8). Our findings provide evidence that FAM129C functions as a potential tumor suppressor under chronic acidic conditions. We propose a therapeutic strategy combining anti-PD-L1 antibody and complement inhibition for the treatment of acid-tolerant tumors. These findings highlight a therapeutic strategy of co-targeting immune checkpoints and the complement pathway in tumors that have adapted to acidic stress and have retained tumorigenic potential.

Limitations of the study

In this study, we demonstrated the mechanisms by which cancer cells evade cell death in acidic tumor microenvironments. However, several limitations should be acknowledged. First, the *in vitro* acidic pH culture system used here could not fully mimic the heterogeneous pH conditions in tumors *in vivo*. Second, validation in human clinical samples would be performed, and the characteristics of the tumor microenvironment in human pancreatic cancer require further investigation. Third, we have not established the immunomodulatory effects of combining anti-PD-L1 therapy with complement inhibitors in clinical studies of pancreatic cancer. Fourth, although we assessed overall immune-cell infiltration, we could not comprehensively characterize the differentiation states and phenotypic heterogeneity of tumor-infiltrating $CD8^+$ T cells, including stemness-associated and exhaustion-associated phenotypes, within the tumor. Further studies incorporating markers related to stemness (e.g., TCF-1, Ly108, and CD62L) and exhaustion markers (e.g., TOX, TIM-3, and LAG-3) would enable a more refined evaluation of $CD8^+$ T cell populations. Addressing these limitations will be essential for translating our findings into therapeutic strategies for pancreatic cancer patients.

RESOURCE AVAILABILITY

Lead contact

Requests for further information, resources, and reagents should be directed to and will be fulfilled by the lead contact, Tsuyoshi Osawa (osawa@onc.rcast.u-tokyo.ac.jp).

Materials availability

This study did not generate new unique reagents.

Data and code availability

- The datasets generated in this study are publicly available in the DDBJ Sequence Read Archive as of the date of publication (RNA-seq raw data, SRA: DRA026488; CRISPR screening sequencing data, SRA: DRA026489; xenograft RNA-seq data, SRA: DRA026490). Direct links to all datasets are provided in the key resources table.
- This paper does not report original code.
- Any additional information required to reanalyze the data reported in this paper is available from the lead contact upon request.

ACKNOWLEDGMENTS

We thank the members of the Division of Nutriomics and Oncology, Laboratory for Systems Biology and Medicine, Genome Science and Medicine, the RCAST, University of Tokyo. We especially thank Dr. T. Tanaka, Dr. T. Kodama, Dr. H. Aburatani, and Dr. A. Nonaka for their helpful discussions and support. We thank Dr. Igor A. Kirilyuk (Vorozhtsov Novosibirsk Institute of Organic Chemistry) for kindly providing the reagents used for EPR imaging in Figure S1D. This work was supported by Grant-in-Aid for Scientific Research (B) (T.O.) and (C) (24K10279, K.Y.), Grant-in-Aid for Transformative Research Areas (A) (25H01339 and 25A304 to T.O.) and (B) (23H03861 to C.I.-Y. and K.Y), Grant-in-Aid for Scientific Research on Innovative Areas (20H04834 to T.O.) and Grants-in-Aid for Challenging Exploratory Research (19K22553, 21K19399, 23K18234, and 25K22572 to T.O.). We also acknowledge support from JSPS KAKENHI grant AdAMS (22H04922) from the Ministry of Education, Culture, Sports, Science and Technology of Japan, the SGH Foundation (T.O.), the Cannon Foundation (T.O.), the Takeda Foundation (T.O.), and the Princess Takamatsu Cancer Foundation (T.O.). This research was also supported by Japan Agency for Medical Research and Development (AMED) under grant numbers JP17cm0106221 and JP19ck0106362 (T.O.). This work was also supported by JST FOREST Program, grant number JPMJFR2306 (T.O.). This study was supported partly by Nanken-Kyoten, TMDU, an Extramural Collaborative Research grant from the Cancer Research Institute, Kanazawa University, and a grant from the Joint Research Program of Institute for Genetic Medicine, Hokkaido University.

AUTHOR CONTRIBUTIONS

T.O. designed research; M.H., B.X., and T.O. designed the experiments; M.H., B.X., K. Maeda, M.S., R.C., S.N., M.N., K. Matsumoto, C.I.-Y., S.A., R.T., H. Yatabe, N.Y., H.H., and S.M. performed the experiments; M.H., B.X., K. Maeda, M.S., F.C., R.C., R.A., S.N., H. Yatabe, M.N., K. Matsumoto, C.I., S.A., K.Y., R.T., S.S., F.K., H. Yanai, N.Y., M.T., H.K., and T.O. analyzed and interpreted data; and M.H., B.X., C.B., A.S., and T.O. wrote the paper.

DECLARATION OF INTERESTS

The authors declare no competing interests.

STAR★METHODS

Detailed methods are provided in the online version of this paper and include the following:

- KEY RESOURCES TABLE

(D) Quantification of cell numbers of $CD8^+$ T cells, IFN-γ^+ $CD8^+$ T cells, $CD11b^+$ cells, $F4/80^+$ cells, and $Ly6G^+$ cells, as well as $CD31^+$ area, in (C). Data are presented as means ± SEM of $n = 15$ biological replicates. Statistical analysis was performed by one-way ANOVA. $^*p < 0.05$, $^{***}p < 0.005$, $^{****}p < 0.001$; ns, not significant.

(E) Graphical summary illustrating the key findings of this study. Under acidic conditions (pH 6.8) that mimic the tumor microenvironment, cancer cells maintained viability and tumor-forming ability even in a floating state. Genes associated with pH resistance were linked to poor prognosis, and the FAM129C-PIGR axis was identified as a key contributor to this resistance. Combination therapy with an anti-PD-L1 antibody and a complement inhibitor exerted synergistic anti-tumor effects against these acid-adapted tumors.

SUPPLEMENTAL INFORMATION

Supplemental information can be found online at https://doi.org/10.1016/j.celrep.2026.117226.

Received: August 14, 2025
Revised: January 30, 2026
Accepted: March 16, 2026

REFERENCES

1. Boedtkjer, E., and Pedersen, S.F. (2020). The Acidic Tumor Microenvironment as a Driver of Cancer. Annu. Rev. Physiol. *82*, 103–126. https://doi.org/10.1146/annurev-physiol-021119-034627.
2. Vaupel, P. (2004). The Role of Hypoxia-Induced Factors in Tumor Progression. Oncologist *9*, 10–17. https://doi.org/10.1634/theoncologist.9-90005-10.
3. García-Jiménez, C., and Goding, C.R. (2019). Starvation and Pseudo-Starvation as Drivers of Cancer Metastasis through Translation Reprogramming. Cell Metab. *29*, 254–267. https://doi.org/10.1016/j.cmet.2018.11.018.
4. Choudhry, H., and Harris, A.L. (2018). Advances in Hypoxia-Inducible Factor Biology. Cell Metab. *27*, 281–298. https://doi.org/10.1016/j.cmet.2017.10.005.
5. Chung, F.-Y., Huang, M.-Y., Yeh, C.-S., Chang, H.-J., Cheng, T.-L., Yen, L.-C., Wang, J.-Y., and Lin, S.-R. (2009). GLUT1 gene is a potential hypoxic marker in colorectal cancer patients. BMC Cancer *9*, 241. https://doi.org/10.1186/1471-2407-9-241.
6. Farina, A.R., Cappabianca, L., Sebastiano, M., Zelli, V., Guadagni, S., and Mackay, A.R. (2020). Hypoxia-induced alternative splicing: the 11th Hallmark of Cancer. J. Exp. Clin. Cancer Res. *39*, 110. https://doi.org/10.1186/s13046-020-01616-9.
7. Dang, C.V. (2009). PKM2 Tyrosine Phosphorylation and Glutamine Metabolism Signal a Different View of the Warburg Effect. Sci. Signal. *2*, pe75. https://doi.org/10.1126/scisignal.297pe75.
8. Zheng, H., and Kang, Y. (2014). Multilayer control of the EMT master regulators. Oncogene *33*, 1755–1763. https://doi.org/10.1038/onc.2013.128.
9. Michl, J., Wang, Y., Monterisi, S., Blaszczak, W., Beveridge, R., Bridges, E.M., Koth, J., Bodmer, W.F., and Swietach, P. (2024). CRISPR-Cas9 screen identifies oxidative phosphorylation as essential for cancer cell survival at low extracellular pH. Cell Rep. *43*, 114499. https://doi.org/10.1016/j.celrep.2024.114499.
10. Warburg, O. (1956). On the Origin of Cancer Cells. Science *123*, 309–314. https://doi.org/10.1126/science.123.3191.309.
11. Barker, J., Khan, M.A.A., and Solomos, T. (1964). Mechanism of the Pasteur Effect. Nature *201*, 1126–1127. https://doi.org/10.1038/2011126a0.
12. Feng, Q., Bennett, Z., Grichuk, A., Pantoja, R., Huang, T., Faubert, B., Huang, G., Chen, M., DeBerardinis, R.J., Sumer, B.D., and Gao, F. (2024). Severely polarized extracellular acidity around tumour cells. Nat. Biomed. Eng. *8*, 787–799. https://doi.org/10.1038/s41551-024-01178-7.
13. Anemone, A., Consolino, L., Arena, F., Capozza, M., and Longo, D.L. (2019). Imaging tumor acidosis: a survey of the available techniques for mapping in vivo tumor pH. Cancer Metastasis Rev. *38*, 25–49. https://doi.org/10.1007/s10555-019-09782-9.
14. Anemone, A., Consolino, L., Conti, L., Irrera, P., Hsu, M.Y., Villano, D., Dastrù, W., Porporato, P.E., Cavallo, F., and Longo, D.L. (2021). Tumour acidosis evaluated in vivo by MRI-CEST pH imaging reveals breast cancer metastatic potential. Br. J. Cancer *124*, 207–216. https://doi.org/10.1038/s41416-020-01173-0.
15. Mi, H., Boehm-Sturm, P., Haeckel, A., Li, Y., Mueller, S., Ni, F., Kratz, H., Foddis, M., Xie, J., and Schellenberger, E. (2025). High-resolution quantitative mapping of extracellular pH by ratiometric MRI with iron chelates in a tumor mouse model. Radiol. Med. *130*, 1231–1242. https://doi.org/10.1007/s11547-025-02020-z.
16. Corbet, C., and Feron, O. (2017). Tumour acidosis: from the passenger to the driver's seat. Nat. Rev. Cancer *17*, 577–593. https://doi.org/10.1038/nrc.2017.77.
17. Kato, Y., Lambert, C.A., Colige, A.C., Mineur, P., Noël, A., Frankenne, F., Foidart, J.-M., Baba, M., Hata, R.-I., Miyazaki, K., and Tsukuda, M. (2005). Acidic Extracellular pH Induces Matrix Metalloproteinase-9 Expression in Mouse Metastatic Melanoma Cells through the Phospholipase D-Mitogen-activated Protein Kinase Signaling. J. Biol. Chem. *280*, 10938–10944. https://doi.org/10.1074/jbc.M411313200.
18. Xu, L., Fukumura, D., and Jain, R.K. (2002). Acidic Extracellular pH Induces Vascular Endothelial Growth Factor (VEGF) in Human Glioblastoma Cells via ERK1/2 MAPK Signaling Pathway: MECHANISM OF LOW pH-INDUCED VEGF. J. Biol. Chem. *277*, 11368–11374. https://doi.org/10.1074/jbc.M108347200.
19. Lee, S.-H., and Griffiths, J.R. (2020). How and Why Are Cancers Acidic? Carbonic Anhydrase IX and the Homeostatic Control of Tumour Extracellular pH. Cancers (Basel) *12*, 1616. https://doi.org/10.3390/cancers12061616.
20. Jäättelä, M. (2004). Multiple cell death pathways as regulators of tumour initiation and progression. Oncogene *23*, 2746–2756. https://doi.org/10.1038/sj.onc.1207513.
21. Zhang, Z., Chen, M., Zhan, W., Chen, Y., Wang, T., Chen, Z., Fu, Y., Zhao, G., Mao, D., Ruan, J., and Yuan, F.-L. (2023). Acid-sensing ion channel 1a modulation of apoptosis in acidosis-related diseases: implications for therapeutic intervention. Cell Death Discov. *9*, 330. https://doi.org/10.1038/s41420-023-01624-6.
22. Xiong, H., Zhai, Y., Meng, Y., Wu, Z., Qiu, A., Cai, Y., Wang, G., and Yang, L. (2024). Acidosis activates breast cancer ferroptosis through ZFAND5/SLC3A2 signaling axis and elicits M1 macrophage polarization. Cancer Lett. *587*, 216732. https://doi.org/10.1016/j.canlet.2024.216732.
23. Zhang, H., Shi, H., Xie, W., Meng, M., Wang, Y., Ma, N., Chang, G., and Shen, X. (2024). Subacute ruminal acidosis induces pyroptosis via the mitophagy-mediated NLRP3 inflammasome activation in the livers of dairy cows fed a high-grain diet. J. Dairy Sci. *107*, 4092–4107. https://doi.org/10.3168/jds.2023-23718.
24. Kondo, A., Yamamoto, S., Nakaki, R., Shimamura, T., Hamakubo, T., Sakai, J., Kodama, T., Yoshida, T., Aburatani, H., and Osawa, T. (2017). Extracellular Acidic pH Activates the Sterol Regulatory Element-Binding

Protein 2 to Promote Tumor Progression. Cell Rep. *18*, 2228–2242. https://doi.org/10.1016/j.celrep.2017.02.006.

25. Kato, M., Maeda, K., Nakahara, R., Hirose, H., Kondo, A., Aki, S., Sugaya, M., Hibino, S., Nishida, M., Hasegawa, M., et al. (2023). Acidic extracellular pH drives accumulation of N1-acetylspermidine and recruitment of protumor neutrophils. PNAS Nexus *2*, pgad306. https://doi.org/10.1093/pnasnexus/pgad306.
26. Rolver, M.G., Camacho-Roda, J., Dai, Y., Flinck, M., Ialchina, R., Hindkær, J., Dyhr, R.T., Bodilsen, A.N., Prasad, N.S., Baldan, J., et al. (2025). Tumor microenvironment acidosis favors pancreatic cancer stem cell properties and *in vivo* metastasis. iScience *28*, 111956. https://doi.org/10.1016/j.isci.2025.111956.
27. Stigliani, A., Ialchina, R., Yao, J., Czaplinska, D., Dai, Y., Andersen, H.B., Rennie, S., Andersson, R., Pedersen, S.F., and Sandelin, A. (2024). Adaptation to an acid microenvironment promotes pancreatic cancer organoid growth and drug resistance. Cell Rep. *43*, 114409. https://doi.org/10.1016/j.celrep.2024.114409.
28. Corbet, C., Pinto, A., Martherus, R., Santiago de Jesus, J.P., Polet, F., and Feron, O. (2016). Acidosis Drives the Reprogramming of Fatty Acid Metabolism in Cancer Cells through Changes in Mitochondrial and Histone Acetylation. Cell Metab. *24*, 311–323. https://doi.org/10.1016/j.cmet.2016.07.003.
29. Böhme, I., and Bosserhoff, A. (2020). Extracellular acidosis triggers a senescence-like phenotype in human melanoma cells. Pigment Cell Melanoma Res. *33*, 41–51. https://doi.org/10.1111/pcmr.12811.
30. Hart, T., Tong, A.H.Y., Chan, K., Van Leeuwen, J., Seetharaman, A., Aregger, M., Chandrashekhar, M., Hustedt, N., Seth, S., Noonan, A., et al. (2017). Evaluation and Design of Genome-Wide CRISPR/SpCas9 Knockout Screens. G3 (Bethesda) *7*, 2719–2727. https://doi.org/10.1534/g3.117.041277.
31. Wang, B., Wang, M., Zhang, W., Xiao, T., Chen, C.-H., Wu, A., Wu, F., Traugh, N., Wang, X., Li, Z., et al. (2019). Integrative analysis of pooled CRISPR genetic screens using MAGeCKFlute. Nat. Protoc. *14*, 756–780. https://doi.org/10.1038/s41596-018-0113-7.
32. Bow, A. (2021). A Streamlined Approach to Pathway Analysis from RNA-Sequencing Data. Methods Protoc. *4*, 21. https://doi.org/10.3390/mps4010021.
33. Biswas, S., Mandal, G., Anadon, C.M., Chaurio, R.A., Lopez-Bailon, L.U., Nagy, M.Z., Mine, J.A., Hänggi, K., Sprenger, K.B., Innamarato, P., et al. (2023). Targeting intracellular oncoproteins with dimeric IgA promotes expulsion from the cytoplasm and immune-mediated control of epithelial cancers. Immunity *56*, 2570–2583.e6. https://doi.org/10.1016/j.immuni.2023.09.013.
34. Chen, C., Xiao, W., Huang, L., Yu, G., Ni, J., Yang, L., Wan, R., and Hu, G. (2017). Shikonin induces apoptosis and necroptosis in pancreatic cancer via regulating the expression of RIP1/RIP3 and synergizes the activity of gemcitabine. Am. J. Transl. Res. *9*, 5507–5517.
35. Shahsavari, Z., Karami-Tehrani, F., Salami, S., and Ghasemzadeh, M. (2016). RIP1K and RIP3K provoked by shikonin induce cell cycle arrest in the triple negative breast cancer cell line, MDA-MB-468: necroptosis as a desperate programmed suicide pathway. Tumour Biol. *37*, 4479–4491. https://doi.org/10.1007/s13277-015-4258-5.
36. Higashi, S., Yamakuchi, M., Hashinokuchi, H., Takenouchi, K., Tabaru, A., Oyama, Y., Fujisaki, C., Tanoue, K., and Hashiguchi, T. (2025). Adaptation to acidic conditions that mimic the tumor microenvironment, downregulates miR-193b-3p, and induces EMT via TGFβ2 in A549 cells. PLoS One *20*, e0318811. https://doi.org/10.1371/journal.pone.0318811.
37. Zhu, S., Zhou, H.-Y., Deng, S.-C., Deng, S.-J., He, C., Li, X., Chen, J.-Y., Jin, Y., Hu, Z.-L., Wang, F., et al. (2017). ASIC1 and ASIC3 contribute to acidity-induced EMT of pancreatic cancer through activating Ca^{2+}/RhoA pathway. Cell Death Dis. *8*, e2806. https://doi.org/10.1038/cddis.2017.189.
38. Roumenina, L.T., Daugan, M.V., Noé, R., Petitprez, F., Vano, Y.A., Sanchez-Salas, R., Becht, E., Meilleroux, J., Clec'h, B.L., Giraldo, N.A., et al. (2019). Tumor Cells Hijack Macrophage-Produced Complement C1q to Promote Tumor Growth. Cancer Immunol. Res. *7*, 1091–1105. https://doi.org/10.1158/2326-6066.CIR-18-0891.
39. Boyd, R.S., Adam, P.J., Patel, S., Loader, J.A., Berry, J., Redpath, N.T., Poyser, H.R., Fletcher, G.C., Burgess, N.A., Stamps, A.C., et al. (2003). Proteomic analysis of the cell-surface membrane in chronic lymphocytic leukemia: identification of two novel proteins, BCNP1 and MIG2B. Leukemia *17*, 1605–1612. https://doi.org/10.1038/sj.leu.2402993.
40. Kadaba, R., Birke, H., Wang, J., Hooper, S., Andl, C.D., Di Maggio, F., Soylu, E., Ghallab, M., Bor, D., Froeling, F.E., et al. (2013). Imbalance of desmoplastic stromal cell numbers drives aggressive cancer processes. J. Pathol. *230*, 107–117. https://doi.org/10.1002/path.4172.
41. Arumugam, P., Bhattacharya, S., Chin-Aleong, J., Capasso, M., and Kocher, H.M. (2017). Expression of polymeric immunoglobulin receptor and stromal activity in pancreatic ductal adenocarcinoma. Pancreatology *17*, 295–302. https://doi.org/10.1016/j.pan.2017.01.013.
42. Kaetzel, C.S. (2005). The polymeric immunoglobulin receptor: bridging innate and adaptive immune responses at mucosal surfaces. Immunol. Rev. *206*, 83–99. https://doi.org/10.1111/j.0105-2896.2005.00278.x.
43. Laumont, C.M., and Nelson, B.H. (2021). IgA transcytosis: A new weapon in the immune response to cancer? Cancer Cell *39*, 607–609. https://doi.org/10.1016/j.ccell.2021.04.007.
44. Arlauckas, S.P., Garris, C.S., Kohler, R.H., Kitaoka, M., Cuccarese, M.F., Yang, K.S., Miller, M.A., Carlson, J.C., Freeman, G.J., Anthony, R.M., et al. (2017). In vivo imaging reveals a tumor-associated macrophage-mediated resistance pathway in anti-PD-1 therapy. Sci. Transl. Med. *9*, eaal3604. https://doi.org/10.1126/scitranslmed.aal3604.
45. Acharya, D., Li, X.R.L., Heineman, R.E.-S., and Harrison, R.E. (2019). Complement Receptor-Mediated Phagocytosis Induces Proinflammatory Cytokine Production in Murine Macrophages. Front. Immunol. *10*, 3049. https://doi.org/10.3389/fimmu.2019.03049.
46. Cavill, R., Kamburov, A., Ellis, J.K., Athersuch, T.J., Blagrove, M.S.C., Herwig, R., Ebbels, T.M.D., and Keun, H.C. (2011). Consensus-phenotype integration of transcriptomic and metabolomic data implies a role for metabolism in the chemosensitivity of tumour cells. PLoS Comput. Biol. *7*, e1001113. https://doi.org/10.1371/journal.pcbi.1001113.
47. Posta, M., and Győrffy, B. (2025). Pathway-level mutational signatures predict breast cancer outcomes and reveal therapeutic targets. Br. J. Pharmacol. *182*, 5734–5747. https://doi.org/10.1111/bph.70215.
48. Komarov, D.A., Ichikawa, Y., Yamamoto, K., Stewart, N.J., Matsumoto, S., Yasui, H., Kirilyuk, I.A., Khramtsov, V.V., Inanami, O., and Hirata, H. (2018). In Vivo Extracellular pH Mapping of Tumors Using Electron Paramagnetic Resonance. Anal. Chem. *90*, 13938–13945. https://doi.org/10.1021/acs.analchem.8b03328.
49. Estrella, V., Chen, T., Lloyd, M., Wojtkowiak, J., Cornnell, H.H., Ibrahim-Hashim, A., Bailey, K., Balagurunathan, Y., Rothberg, J.M., Sloane, B.F., et al. (2013). Acidity generated by the tumor microenvironment drives local invasion. Cancer Res. *73*, 1524–1535. https://doi.org/10.1158/0008-5472.CAN-12-2796.
50. Tamura, I., Sakamoto, D.M., Yi, B., Saito, Y., Yamada, N., Morimoto, J., Takakusagi, Y., Kuroda, M., Kubota, S.I., Yatabe, H., et al. (2024). Click3D: Click reaction across deep tissues for whole-organ 3D fluorescence imaging. Sci. Adv. *10*, eado8471. https://doi.org/10.1126/sciadv.ado8471.
51. Schindelin, J., Arganda-Carreras, I., Frise, E., Fiji, et al. (2012). An open-source platform for biological-image analysis. Nat. Methods *9*, 676–682. https://doi.org/10.1038/nmeth.2019.
52. Tamura, A., Yamagata, K., Kono, T., Fujimoto, M., Fuchigami, T., Nishimura, M., Yokoyama, M., Nakayama, A., Hashimoto, N., Sakuma, I., et al. (2025). p53-inducible lncRNA LOC644656 causes genotoxic stress-induced stem cell maldifferentiation and cancer chemoresistance. Nat. Commun. *16*, 4818. https://doi.org/10.1038/s41467-025-59886-w.

53. Xie, Z., Bailey, A., Kuleshov, M.V., Clarke, D.J.B., Evangelista, J.E., Jenkins, S.L., Lachmann, A., Wojciechowicz, M.L., Kropiwnicki, E., Jagodnik, K.M., et al. (2021). Gene Set Knowledge Discovery with Enrichr. Curr. Protoc. *1*, e90. https://doi.org/10.1002/cpz1.90.

54. Sanson, K.R., Hanna, R.E., Hegde, M., Donovan, K.F., Strand, C., Sullender, M.E., Vaimberg, E.W., Goodale, A., Root, D.E., Piccioni, F., and Doench, J.G. (2018). Optimized libraries for CRISPR-Cas9 genetic screens with multiple modalities. Nat. Commun. *9*, 5416. https://doi.org/10.1038/s41467-018-07901-8.

55. Li, W., Xu, H., Xiao, T., Cong, L., Love, M.I., Zhang, F., Irizarry, R.A., Liu, J.S., Brown, M., and Liu, X.S. (2014). MAGeCK enables robust identification of essential genes from genome-scale CRISPR/Cas9 knockout screens. Genome Biol. *15*, 554. https://doi.org/10.1186/s13059-014-0554-4.

56. Sápi, J., Kovács, L., Drexler, D.A., Kocsis, P., Gajári, D., and Sápi, Z. (2015). Tumor Volume Estimation and Quasi-Continuous Administration for Most Effective Bevacizumab Therapy. PLoS One *10*, e0142190. https://doi.org/10.1371/journal.pone.0142190.

57. Győrffy, B. (2024). Integrated analysis of public datasets for the discovery and validation of survival-associated genes in solid tumors. Innovation *5*, 100625. https://doi.org/10.1016/j.xinn.2024.100625.

58. Bartha, Á., and Győrffy, B. (2021). TNMplot.com: A Web Tool for the Comparison of Gene Expression in Normal, Tumor and Metastatic Tissues. Int. J. Mol. Sci. *22*, 2622. https://doi.org/10.3390/ijms22052622.

STAR★METHODS

KEY RESOURCES TABLE

REAGENT or RESOURCE	SOURCE	IDENTIFIER
Antibodies		
FAM129C	Abcam	#ab113755
PIGR	Abcam	#ab96196; RRID: AB_10677612
β-actin	Sigma-Aldrich	#A5441; RRID: AB_476744
GPX4	Cell Signaling Technology	#52455; RRID: AB_2924984
RIP	Cell Signaling Technology	#3493; RRID: AB_2305314
phospho-RIP	Cell Signaling Technology	#65746; RRID: AB_2799693
MLKL	Cell Signaling Technology	#14993; RRID: AB_2721822
phospho-MLKL	Cell Signaling Technology	#91689; RRID: AB_2732034
cleaved Caspase-3	Cell Signaling Technology	#9661S; RRID: AB_2341188
Caspase-3	Cell Signaling Technology	#9662S; RRID: AB_331439
GSDMD	Cell Signaling Technology	#97558S; RRID: AB_2864253
ZEB1	Cell Signaling Technology	#D80D3; RRID: AB_1904164
E-cadherin	Cell Signaling Technology	#24E10; RRID: AB_2291471
Vimentin	Cell Signaling Technology	#D21H3; RRID: AB_10695459
Snail	Cell Signaling Technology	#C15D3; RRID: AB_2255011
C3	Cell Signaling Technology	#97425; RRID: AB_2313773
C5a	Abcam	#202039; RRID: AB_2313773
donkey anti-mouse IgG	Sigma-Aldrich	#A4416; RRID: AB_2075239
anti-rabbit	Cell Signaling Technology	#7074P2; RRID: AB_2099233
CD16/32	BioLegend	#101301; RRID: AB_312800
CD4	BD Biosciences	#565634; RRID: AB_2739312
CD8	BD Biosciences	#565968; RRID: AB_2739421
CD11b	BioLegend	#101227; RRID: AB_393577
I-A/I-E	BD Biosciences	#745580; RRID: AB_2743096
B220	BD Biosciences	#17045282; RRID:AB_469395
Ly6C	BioLegend	#128007; RRID: AB_1186133
CD11c	BD Biosciences	#565451; RRID: AB_2744278
NK1.1	BioLegend	#156537; RRID: AB_3083138
F4/80	BioLegend	#123107; RRID: AB_893500
Ly6G	BD Biosciences	#746448; RRID: AB_2743751
CD45	BD Biosciences	#557659; RRID: AB_396774
APC-conjugated PD-1	BioLegend	#135210; RRID: AB_2159183
Brilliant Violet 421-conjugated KLRG1	BioLegend	#138413; RRID:AB_10918627
APC-Cy7-conjugated CD44	BioLegend	#103027; RRID: AB_830784
PerCP-Cy5.5-conjugated CD62L	BioLegend	#104431; RRID:AB_2187123
PE-Cy7-conjugated Sca-1	BioLegend	#108113; RRID: AB_493597
FITC-conjugated CD122	BioLegend	#123207; RRID: AB_940611
anti-rat CD11b	BD Biosciences	#550282; RRID: AB_393577
anti-hamster CD31	Millipore	#MAB1398Z; RRID: AB_94207
rat anti-mouse F4/80	Bio-Rad	#MCA497GA; RRID: AB_323806
rat anti-mouse Ly-6G	BioLegend	#127602; RRID: AB_1089180
Anti-MLKL (phospho S358) antibody	Abcam	ab187091; RRID: AB_2619685
Alexa Fluor 488-conjugated goat anti-rat	Thermo Fisher Scientific	#A11006; RRID: AB_2534074

(*Continued on next page*)

Please cite this article in press as: Hasegawa et al., Tolerance to extracellular acidic pH facilitates tumor plasticity, Cell Reports (2026), https://doi.org/10.1016/j.celrep.2026.117226

Continued

REAGENT or RESOURCE	SOURCE	IDENTIFIER
Alexa Fluor 568-conjugated goat anti-hamster	Iwai Chemicals	#127-165-160; RRID: AB_2535761
Alexa Fluor 488-conjugated goat anti-rabbit	Thermo Fisher Scientific	#A11034; RRID: AB_2576217
PerCP-Cy5.5 anti-CD8	BioLegend	#100733; RRID: AB_2075239
Alexa Fluor 647 anti-mouse IFN-γ	BioLegend	#505816; RRID: AB_493315
anti-mouse PD-L1	Selleck	#A2115; RRID: AB_3675704
Bacterial and virus strains		
DH5α	Thermo Fisher Scientific	#18258012
Chemicals, peptides, and recombinant proteins		
DMEM (High Glucose)	Nacalai Tesque	#08459-64
RPMI 1640 Medium	Nacalai Tesque	#30264-56
Fetal bovine serum	Nissui	#174012
7-Cl-O-Nec1	Abcam	#ab221984
zVAD-FMK	BD Biosciences	#305664
Necrostatin-1	Enzo Life Sciences	#BML-AP309-0020
Ferrostatin-1	MedChemExpress	#HY-100579
cOmplete™ Protease Inhibitor Cocktail (1×)	Roche	#11697498001
Chemi-Lumi One Ultra	Nacalai Tesque	#02230-54
Isogen reagent	Nippon Gene	#311-02501
PrimeScript™ reverse transcriptase	Takara	#RR037A
THUNDERBIRD® SYBR® qPCR Mix	Toyobo	#QPS-201
Sepasol®-RNA I Super G	Nacalai Tesque	#09379-55
Polybrene	Sigma-Aldrich	#H9268
4% paraformaldehyde	FUJIFILM Wako	#163-20145
Acetone	Nacalai Tesque	#00529-85
Puromycin	InvivoGen	#ant-pr-1
RBC Lysis Buffer	Invitrogen	#00-4333-57
Dako Protein Block, Serum-free	Agilent	#X090930-2
DAPI-Fluoromount-G	Southern Biotech	#0100-20
Dextran, SNARF™-1, 70,000 MW, Anionic	Invitrogen	D3304
Pimo-yne	Dr. Sando, University of Tokyo	N/A
PMX53	Selleck	#S6293
Critical commercial assays		
Calcein AM (Ex/Em = 480/515 nm)	Thermo Fisher Scientific	#C3099
LDH Cytotoxicity Detection Kit	Nacalai Tesque	#289-97301
MiSeq v2 Reagent Kit	Illumina	#MS-102-2002
NucleoSpin Tissue Kit	Takara	#740952.50
Human Complement C3a ELISA Kit	Invitrogen	BMS2089
Human Complement C5a ELISA Kit	Invitrogen	BMS2088
KAPA HiFi HotStart ReadyMix	KAPA Biosystems	#KK2602
FastGene Gel/PCR Extraction Kit	Nippon Genetics	#FG-91202
Experimental models: Cell lines		
PANC1	ATCC	CRL-1469
MIA-PaCa2	ATCC	CRL-1420
HeLa	ATCC	CCL-2
HSML	Dr. Kudoh, Hirosaki University, Japan	N/A
HEK293T	ATCC	CRL-11268

(*Continued on next page*)

Please cite this article in press as: Hasegawa et al., Tolerance to extracellular acidic pH facilitates tumor plasticity, Cell Reports (2026), https://doi.org/10.1016/j.celrep.2026.117226

Continued

REAGENT or RESOURCE	SOURCE	IDENTIFIER
Plat-GP	Cosmo Bio Co., LTD.	PVK-302
Pan02	Dr. Yamauchi, Kawasaki Medical School, Japan	N/A
Deposited data		
Deposited data	N/A	https://ddbj.nig.ac.jp/search?query=%22PRJDB40299%22
RNA-seq raw data	This paper	SRA: DRA026488 (https://www.ncbi.nlm.nih.gov/sra/?term=DRA026488)
CRISPR screening sequencing data	This paper	SRA: DRA026489 (https://www.ncbi.nlm.nih.gov/sra/?term=DRA026489)
Xenograft RNA-seq	This paper	SRA: DRA026490 (https://www.ncbi.nlm.nih.gov/sra/?term=DRA026490)
Experimental models: Organisms/strains		
C57BL/6J mice (male)	CLEA Japan, Inc.	Cat# C57BL/6NJcl RRID: IMSR_JCL:C57BL/6NJcl
C.B-17/Icrscid/scid Jcl mice (male)	CLEA Japan, Inc.	Cat# C.B-17/Icr-scid/scidJcl RRID: IMSR_JCL:C.B-17/Icr-scid/scidJcl
Oligonucleotides		
Primers for real-time PCR, see Table S1	This paper	N/A
Recombinant DNA		
Toronto KnockOut (TKO) CRISPR Library v3	Addgene	Plasmid #90294
psPAX2	Addgene	Plasmid #12260
pMD2.G	Addgene	Plasmid #12259
lentiCRISPR v2	Addgene	Plasmid #52961
pMx puro-FAM129C	This paper	N/A
pMx puro-PIGR	This paper	N/A
Software and algorithms		
FastQC v0.11.9	Babraham Bioinformatics	https://www.bioinformatics.babraham.ac.uk/projects/fastqc/
Trimmomatic v0.39	Usadel Lab	http://www.usadellab.org/cms/?page=trimmomatic
HISAT2 v2.2.1	Kim Lab	https://daehwankimlab.github.io/hisat2/
featureCounts v2.0.3	Subread package	http://subread.sourceforge.net/
EnhancedVolcano	Bioconductor	https://github.com/kevinblighe/EnhancedVolcano
TCC	Bioconductor	https://bioconductor.org/packages/TCC/
Enrichr	Ma'ayan Lab	https://maayanlab.cloud/Enrichr/
IMPaLa	Cavill et al.[46]	http://impala.molgen.mpg.de/
gplots	CRAN	https://cran.r-project.org/package=gplots
Kaplan-Meier Plotter	Posta and Győrffy[47]	http://kmplot.com/analysis/
MAGeCK-Flute v0.5.8	Li Lab	https://sourceforge.net/p/mageck/wiki/Home/
FACSDiva software v9.0	BD Biosciences	N/A
FlowJo software v10.2	BD Biosciences	https://www.flowjo.com
LAS X software v4.2.1	Leica Microsystems	N/A
Fiji (ImageJ)	Schindelin et al., 2012	https://fiji.sc
GraphPad Prism v9.2.0	Dotmatics	https://www.graphpad.com/
R version 4.3.3	The Comprehensive R Archive Network	https://cran.r-project.org/
Other		
Confocal microscope (STELLARIS 5)	Leica Microsystems	N/A

(*Continued on next page*)

Please cite this article in press as: Hasegawa et al., Tolerance to extracellular acidic pH facilitates tumor plasticity, Cell Reports (2026), https://doi.org/10.1016/j.celrep.2026.117226

Continued

REAGENT or RESOURCE	SOURCE	IDENTIFIER
Cytation 5 multimode plate reader	BioTek Instruments, Winooski, VT, USA	N/A
ARVO microplate reader	PerkinElmer, Waltham, MA, USA	N/A
Fusion FX imaging system	Vilber Lourmat	N/A
LSRFortessa™ Flow Cytometer	BD Biosciences	N/A
Cryostat CM1950	Leica Microsystems	N/A

EXPERIMENTAL MODEL AND STUDY PARTICIPANT DETAILS

Cell lines

Human pancreatic carcinoma cell lines PANC1 and MIA-PaCa2, along with the human cervical cancer cell line HeLa, were sourced from the American Type Culture Collection (ATCC, Manassas, VA, USA). The mouse pancreatic cancer cell line Pan02 was obtained from Dr. Kuribayashi (Kawasaki Medical School, Japan). The mouse cervical cancer cell line HSML was obtained from Dr. Kudoh (Hirosaki University, Japan). Cells were cultivated in Dulbecco's modified Eagle's medium (DMEM) (Nacalai Tesque, Kyoto, Japan) with 10% fetal bovine serum (FBS) under standard conditions (37°C, 5% CO_2), except for PANC1, HSML, and Pan02 cells, which were maintained in RPMI 1640 medium (Nacalai Tesque, Kyoto, Japan). All human cell lines were authenticated by short tandem repeat (STR) profiling by the supplier (ATCC). Cell lines were routinely tested for mycoplasma contamination using PCR-based detection methods and were confirmed to be negative.

Animals

Male C57BL/6 mice and C.B-17/Icr-scid/scidJcl mice aged 8 weeks were purchased from CLEA Japan, Inc. The animals were housed in individual cages in a temperature- and light-controlled environment and had *ad libitum* access to chow and water. All mouse experiments were approved by the University of Tokyo Animal Care and Use Committee. Only female mice were used in this study. Therefore, potential sex-based differences were not evaluated and represent a limitation of this study.

METHOD DETAILS

Acidic pH cell culture conditions

To simulate acidic environments (pH 5.6 or 6.8), the concentration of sodium bicarbonate was reduced or hydrochloric acid (HCl) was supplemented to Dulbecco's Modified Eagle Medium (DMEM; Nissui, Tokyo, Japan). Autoclaved base DMEM was supplemented with 10% fetal bovine serum (FBS) and 584 mg/L L-glutamine. Sodium bicarbonate was then added at a final concentration of 6.86 mM to prepare the pH 7.4 medium, or at 1.72 mM to prepare the pH 6.8 medium. For the pH 5.6 medium, sodium bicarbonate (6.86 mM final) and 6 M HCl (9.0 mM final) were added. The pH of each medium was confirmed to be stable for at least 24 h under 5% CO_2 at 37°C.

Unless otherwise noted, cells were cultured under each pH condition for 24 h prior to downstream assays. For the LDH assay and the inhibitor-treated cell viability assay shown in Figures 1G and 1H, cells were incubated at the indicated pH for 6 h before analysis.

For the RT–qPCR analyses shown in Figures 3A and 3B, cells were cultured under chronic acidic conditions. Specifically, PANC1 cells were maintained at pH 6.8 for 14 days; during this period, 24-h recovery cultures at pH 7.4 were intermittently introduced to maintain sufficient cell numbers.

After culture under each condition, unless otherwise indicated, adherent and floating cells were collected together. When specified, cells were fractionated and collected separately as adherent ("ad") or floating ("fl") populations.

In vivo pH mapping by EPR

In vivo pH mapping was performed using continuous-wave EPR imaging, as previously described by Komarov et al.[48] Briefly, MIA-PaCa2 and SU.86.86-bearing mice were anesthetized with isoflurane, and the pH-sensitive nitroxyl radical dR-SG was injected intravenously via the tail vein. EPR imaging was initiated 2 min after probe injection under temperature- and respiration-controlled conditions.

Ratiometric measurements of tumor pHe

Tumor extracellular pH (pHe) was measured using the radiometric fluorescent pH indicator Dextran, SNARF-1, 70,000 MW, anionic (Invitrogen, D3304), based on the method described by Estrella et al.[49] with minor modifications.

SNARF-1 Dextran was administered via tail vein injection at 44 mg/kg to SCID mice bearing MIA PaCa-2 tumors (~1,000 mm^3). Four hours after injection, mice were euthanized, and tumors were immediately harvested, embedded, and processed for frozen sectioning. Tissue sections were mounted with DAPI-containing mounting medium and imaged using a confocal microscope (STELLARIS 5, Leica Microsystems).

SNARF-1 fluorescence was detected at emission wavelengths corresponding to the acidic (580 nm) and alkaline (640 nm) forms of the dye. Images were acquired from both the tumor core and periphery (n = 5 fields per region). Ratiometric images were generated, and pHe values were calculated from fluorescence intensity ratios using *in vitro* calibration curves. Conversion of intensity ratios to pH values was performed using the equation described previously.[49]

In vivo hypoxia imaging

Pimo-yne,[50] provided by the Sando Laboratory, was used for hypoxia labeling. Experiments were performed in SCID mice bearing MIA PaCa-2 tumors or C57BL/6 mice bearing Pan02 tumors, each with an approximate tumor volume of 1,000 mm^3. Pimo-yne was prepared at a concentration of 6 mg/mL in vehicle (5% DMSO, 45% PEG400, and 50% PBS) and administered to mice at a dose of 5 μL per gram of body weight.

Two hours after Pimo-yne administration, mice were euthanized, and tumors were immediately harvested and processed for frozen sectioning. Tumor sections were subjected to click chemistry labeling using a reaction mixture containing 25 μM Cy5-dye-azide, 1 mM $CuSO_4$, 2 mM BTTAA, and 5 mM sodium ascorbate (NaAsc) in 10% DMSO/PBS and incubated at room temperature for 1 h.

After labeling, sections were washed three times with PBS containing 0.2% Triton X-100 (10 min each), followed by blocking with DAKO Protein Block at room temperature for 30 min. Sections were then washed three times with PBS-T, mounted with DAPI-containing mounting medium, and imaged by fluorescence microscopy. Images were acquired from both the tumor core and periphery, with three fields analyzed per region (n = 3).

Excitation for Cy5 and DAPI was provided by a 633- and 405-nm laser, respectively. Cy5-positive areas were determined with Fiji software.[51] Each positive area was binarized and quantified using the Analyze Particle tool. 3 or 5 random fields per section were imaged.

Live-cell staining, confocal time-lapse imaging, and image analysis

MIA-PaCa2 cells were stained with Calcein AM (Thermo Fisher Scientific, Waltham, MA, USA; excitation/emission: 480/515 nm) at a final concentration of 1 μg/mL in PBS for 30 min at 37°C. After staining, cells were washed twice with PBS, and the medium was replaced with pH-adjusted culture media (pH 7.4, 6.8, or 5.6). Time-lapse imaging was then performed using a confocal microscope (STELLARIS 5, Leica Microsystems) at 5-min intervals.

Cell lysis, membrane rupture, and LDH release

Cell lysis and membrane rupture were evaluated by measuring lactate dehydrogenase (LDH) activity in the extracellular medium using an LDH Cytotoxicity Detection Kit (Nacalai Tesque, Kyoto, Japan), following the manufacturer's instructions. PANC1, MIA-PaCa2, and HeLa cells were seeded into 96-well plates at a density of 6.0×10^4 cells per well and cultured for 24 h. The cells were then incubated for an additional 24 h in culture media adjusted to pH 7.4, 6.8, or 5.6. Following incubation, LDH release was quantified. The absorbance of the medium alone was subtracted as background, and LDH release at each pH condition was normalized to the value at pH 7.4 to determine the relative LDH release.

For the inhibitor treatment shown in Figure 1G, 7-Cl-*O*-Nec1 (a metabolically stable RIP1 inhibitor; Abcam, ab221984) was used at a final concentration of 50 μM. Cells were pre-incubated with Nec1 in standard medium for 1 h before pH adjustment. The pH-adjusted media also contained Nec1 at the same final concentration (50 μM), and cells were cultured under these conditions for 6 h. LDH activity was monitored using a Cytation 5 multimode plate reader (BioTek Instruments, Winooski, VT, USA).

Cell viability assay

Cells were suspended in either control (pH 7.4) or acidic culture medium (pH 6.8 or 5.6), then seeded at a density of 6×10^3 cells per well into 96-well flat-bottom microtiter plates (100 μL per well), and incubated overnight at 37°C. Cell viability was assessed using the sulforhodamine B (SRB) assay. Briefly, cells were fixed with 10% (w/v) trichloroacetic acid, stained with 0.4% (w/v) SRB in 1% acetic acid, washed, and air-dried. Subsequently, 100 μL of 10 mM Tris base solution (pH ~10.5) was added to each well and incubated at room temperature for 20 min. Absorbance was measured at 570 nm using an ARVO microplate reader (PerkinElmer, Waltham, MA, USA).

In Figures 1D–1H, cells were cultured under the indicated pH conditions (pH 7.4, 6.8, or 5.6) for 24 h prior to viability assessment. For Nec1 treatment (7-Cl-*O*-Nec1, a metabolically stable RIP1 inhibitor; Abcam, ab221984), cells were pre-incubated with Nec1 at a final concentration of 50 μM for 1 h before medium replacement. The pH-adjusted media also contained 50 μM Nec1, and cells were then cultured for an additional 24 h.

In Figure S1F, zVAD-FMK (BD Biosciences, BD305664), Necrostatin-1 (Enzo Life Sciences, BML-AP309-0020), and Ferrostatin-1 (MedChemExpress, HY-100579) were dissolved in DMSO and administered accordingly. Culture medium was removed from each

Please cite this article in press as: Hasegawa et al., Tolerance to extracellular acidic pH facilitates tumor plasticity, Cell Reports (2026), https://doi.org/10.1016/j.celrep.2026.117226

well, and 100 μL of drug-containing medium was added. Six replicates were prepared for each drug concentration. Plates were incubated for 1 h at 37°C. After drug exposure, the medium was replaced with fresh complete growth medium, and cells were further incubated for 3 days. Cell viability was assessed every 24 h.

Immunoblotting

Cells were cultured under the indicated pH conditions for 24 h or treated with cisplatin (final concentration: 33.3 μM) for 24 h. For the immunoblotting shown in Figure 2D, after incubation under each pH condition, cells were separated into adherent (ad) and floating (fl) populations before lysis.

Cells were lysed in RIPA buffer (50 mM Tris-HCl pH 7.5, 150 mM NaCl, 0.5% SDS, 1% NP-40, 2 mM EDTA, and 1× cOmplete Protease Inhibitor Cocktail (Roche)) and incubated on ice for 30 min. Lysates were centrifuged at 15,000 rpm for 10 min, and the supernatants were collected for protein quantification using the Bio-Rad Protein Assay. Equal amounts of protein were denatured in SDS sample buffer, resolved by 10% SDS-PAGE, and transferred to nitrocellulose membranes at 100 V for 1.5 h.

Membranes were blocked with 5% skim milk in TBS-T for 1 h at room temperature (approximately 25°C) and incubated overnight at 4°C with the following primary antibodies:

anti-FAM129C (Abcam, #ab113755), anti-PIGR (Abcam, #ab96196), anti-β-actin (Sigma-Aldrich, #A5441), anti-GPX4 (CST, #52455), anti-RIP (CST, #3493), anti-phospho-RIP (CST, #65746), anti-MLKL (CST, #14993), anti-phospho-MLKL (CST, #91689), anti-cleaved Caspase-3 (CST, #9661S), anti-Caspase-3 (CST, #9662S), anti-GSDMD (CST, #97558S), anti-ZEB1 (CST, #D80D3), anti-E-cadherin (CST, #24E10), anti-Vimentin (CST, #D21H3), anti-Snail (CST, #C15D3), anti-C3 (CST, #97425), and anti-C5 (Abcam, # ab202039).

After three washes in TBS-T, membranes were incubated for 1 h at room temperature (approximately 25°C) with HRP-conjugated secondary antibodies: donkey anti-mouse IgG (Sigma-Aldrich, #A4416) or anti-rabbit IgG (CST, #7074P2). After an additional three washes, signal detection was performed using Chemi-Lumi One Ultra (Nacalai), and images were acquired with Fusion FX (VILBER).

Quantitative real-time PCR

The total RNA of cells was isolated using Isogen reagent (Nippon Gene) and converted to cDNA using PrimeScript reverse transcriptase (Takara) in accordance with the manufacturer's instructions. The converted cDNA was subsequently utilized for quantitative real-time PCR amplification with Thunderbird SYBR Green qPCR Mix (Toyobo) and primers (Table S1). mRNA expression levels were then normalized to *ACTB*. The threshold cycle (CT) was used to estimate the amount of target mRNA. The comparative CT method with the formula for relative fold-change = $2^{-\Delta\Delta CT}$ was used to quantify the amplified transcripts.

Quantification of floating cells

PANC1 and MIA-PaCa2 cells were seeded into 6-cm dishes at densities of 1.0×10^6 and 3.0×10^6 cells per dish, respectively, and incubated under standard conditions for 24 h. The medium was then replaced with medium adjusted to pH 7.4, pH 6.8, or pH 5.6, and cells were further incubated for an additional 24 h. Subsequently, floating and adherent cells were collected and counted separately. The percentage of floating cells was calculated relative to the total number of cells.

Assessment of cell adhesiveness

PANC1 and MIA-PaCa2 cells were seeded into 10-cm dishes at a density of 5.0×10^6 cells per dish and cultured for 24 h. The culture medium was then replaced with medium adjusted to pH 6.8 or pH 5.6, followed by an additional 24-h incubation. Floating cells were subsequently collected and reintroduced into medium adjusted to either pH 7.4 or pH 6.8 and cultured for an additional 48 h. Cell viability was assessed using the SRB assay, and absorbance values were normalized to evaluate the relative number of adherent viable cells.

Enzyme-linked immunoassay (ELISA)

Levels of human C3a and C5a were measured using commercially available ELISA kits (Human C3a ELISA Kit, BMS2089; Human C5a ELISA Kit, BMS2088; Thermo Fisher Scientific) according to the manufacturer's instructions.

Cells cultured under acidic (pH 6.8) or physiological (pH 7.4) conditions were separated into adherent or floating fractions. Each fraction was lysed using an SDS-free lysis buffer, and the resulting cell lysates were subjected to ELISA analysis.

RNA-sequencing data analysis

Excised mouse tumors were homogenized at 2800 rpm in Sepasol-RNA I Super G (Nakalai) and lysed by sonication. RNA was extracted following the manufacturer's protocol. Extracted RNA was denatured with HT1 Hyb Buffer 1 and 1M NaOH at 25°C for 5 min and subjected to RNA sequencing using the MiSeq v2 Reagent Kit (Illumina). Quality control of the 300 bp paired-end reads was performed using FastQC, and sequence trimming was conducted with Trimmomatic. Reads were mapped to the reference genome (hg38) with HISAT2, and raw read counts for each gene were calculated using featureCounts. Expression levels (FPKM and TPM) were computed from the fragments counted by featureCounts. RNA from three independent tumor samples per group (control and comparison) was analyzed. Volcano plots of TPM values were generated using the EnhancedVolcano package in R. Genes with a p value < 0.05 and more than a 2-fold decrease in expression were subjected to pathway analysis using IMPaLA (version

13).[46] DEGs were performed using a method outlined in a previous study.[52] In brief, DEGs were identified using R (TCC library)/Bioconductor software (version 4.0.4; FDR < 0.05, |log2FC| > 1). Calculated DEGs were used for the downstream analysis, such as Gene Ontology analysis and TRRUST analysis by Enrichr (https://maayanlab.cloud/Enrichr/)[53] as a hub for further GO analyses. In addition, dot plots and a heatmap with a dendrogram were generated using R software (gplots).

gRNA screening

HEK293T cells were seeded into 15-cm dishes and transfected with the Toronto KnockOut (TKO) CRISPR Library Version 3, pMD2.G, and psPAX2 using a standard calcium phosphate or lipofection method. Culture supernatants were collected 24 h after transfection, centrifuged at 1,000 rpm for 5 min, supplemented with 0.1 μg/mL polybrene, and filtered through a 0.45 μm membrane to prepare lentiviral supernatants.

PANC1 cells were seeded into 6-well plates at a density of 3×10^6 cells per well and infected with 400 μL of viral supernatant per well (multiplicity of infection [MOI] = 0.3). After 24 h, cells were transferred to 10-cm dishes and selected with 2 μg/mL puromycin for 7 days. On day 15 post-infection, puromycin was removed, and cells were cultured in pH-adjusted media. For each pH condition, cells were distributed into forty 15-cm dishes.

Under the pH 7.4 condition, cells were continuously cultured for 24 days. Under the pH 6.8 condition, in order to maintain sufficient cell numbers, the culture medium was temporarily switched to normal-pH (pH 7.4) on days 3, 9, and 19 and reverted to acidic-pH (pH 6.8) after 3 days. Passaging was performed twice during the normal-pH periods and once during acidic-pH culture to maintain a total of $\geq 2.4 \times 10^8$ cells, thereby ensuring a coverage of ≥1000 cells per sgRNA throughout the screening.

Genomic DNA was extracted from cells cultured under acidic pH conditions on days 0 and 24 using the NucleoSpin Tissue Kit (Takara). Amplification of sgRNA cassettes was performed according to the TKOv3 protocol (Addgene), using 2.5 μg of gDNA per 50 μL PCR reaction with the KAPA HiFi Reaction Mix (KAPA Biosystems). PCR products were separated on 1% agarose gels, and the appropriate bands were excised and purified using the Fast Gene Gel/PCR Extraction Kit (NIPPON Genetics).

The resulting libraries were sequenced using the MiSeq v2 Reagent Kit (Illumina) to quantify sgRNA abundance. Sequencing reads were demultiplexed and processed using the MAGeCK Flute pipeline (v0.5.8), which performed read alignment to the TKOv3 reference library (Addgene) in count mode, followed by normalization and identification of significantly enriched or depleted sgRNAs using the test module in RRA mode. Day 0 samples served as controls, and day 24 samples as experimental conditions. The analysis was conducted in "control" mode, which performs normalization using non-targeting control sgRNAs.[54]

Gene-level significance was evaluated using the Robust Rank Aggregation (RRA) algorithm implemented in MAGeCK. The RRA score integrates the ranks of multiple sgRNAs targeting each gene to estimate the likelihood that the gene is significantly selected under the screening condition. Lower RRA scores indicate higher statistical confidence in the gene's involvement.[55]

Generation of knockout and overexpression cell lines

sgRNAs targeting *FAM129C* (sequences: #1 GAGCCGAGGAACGCAGGCGG; #2 AAGGCAGGAAGTTCCTCAGC) were extracted from the TKOv3 library and cloned into CRISPRv2 backbones. Constructs (empty vector, *FAM129C*-targeting sgRNA vectors #1 and #2, or pMx puro with FAM129 or PIGR cDNA), along with pMD2.G and psPAX2, were transfected into HEK293T cells. After transfection, culture supernatants were collected, centrifuged at 1000 rpm for 5 min, supplemented with polybrene (0.1 μg/mL), and filtered (0.45 μm) to produce viral supernatants. PANC1, MIA-PaCa2, Pan02, and HSML cells were infected and selected with 2 μg/mL puromycin for 1 week. For knockout cell lines, PANC1 and Pan02 cells were plated in 96-well plates at limiting dilution to obtain single-cell-derived colonies, which were subsequently expanded and cloned.

Fluorescence-activated cell sorting (FACS)

Tumor-derived cells were enzymatically dissociated at 37°C for 1 h with gentle agitation (180 rpm) in a digestion buffer containing collagenase (0.75 μg/mL; Roche), DNase I (40 μg/mL; Roche), and dispase (0.5 μg/mL; Thermo Fisher Scientific). The resulting cell suspensions were passed through a 40 μm BD Falcon strainer to remove debris and aggregates, followed by red blood cell (RBC) lysis using an RBC lysis buffer (Invitrogen). After washing with PBS, cells were incubated with anti-CD16/32 antibody (BioLegend) on ice for 5 min to block Fc receptors.

For surface marker staining, cells were incubated for 20 min on ice in PFE buffer (PBS supplemented with 2% FBS and 1 mM EDTA) with fluorochrome-conjugated antibodies against the following markers: CD4 (RM4-5; BV480), CD8 (53-6.7; BUV395), CD11b (M1/70; PerCP-Cy5.5), I-A/I-E (25-9-17; BUV395), B220 (RA3-6B2; APC), Ly6C (HK1.4; PE), CD11c (N418; BV421), NK1.1 (S17016D; BV421), F4/80 (BM8; FITC), Ly6G (1A8; BV480), CD45 (30-F11; APC-Cy7), PD-1 (29F.1A12; APC), CD44 (IM7; APC-Cy7), CD62L (MEL-14; PerCP-Cy5.5), Sca-1 (D7; PE-Cy7), and CD122 (TM-β1; FITC). Using these panels, T cell exhaustion and stemness, as well as macrophage polarization, were quantified by flow cytometry (FACS). Antibodies were purchased from BioLegend or BD Biosciences, as indicated.

Where applicable, viability dye staining was performed to exclude dead cells. After staining, cells were washed and analyzed using a BD LSR Fortessa flow cytometer (BD Biosciences). Data were acquired with FACSDiva software (BD Biosciences) and analyzed using FlowJo software (v10.2; BD Biosciences). Gating strategies are provided in Figure 5L. Quantification was performed using samples from four independent tumors ($n = 4$).

Please cite this article in press as: Hasegawa et al., Tolerance to extracellular acidic pH facilitates tumor plasticity, Cell Reports (2026), https://doi.org/10.1016/j.celrep.2026.117226

Immunohistochemistry analysis of tumor tissue

Tumors were isolated, directly embedded in optimal cutting temperature (OCT) compound, and stored at −80°C until analysis. Frozen tumor tissues were cut 15 μm thick by using Cryostat CM1950 (Leica). For pMLKL, CD11b, F4/80, Ly6G, and CD31 staining, tissues were fixed with 4% PFA for 10 min at room temperature, blocked by Dako Protein Block (serum-free, X0909, Agilent Technologies) for 30 min at room temperature, and stained with antibodies against pMLKL (Abcam, ab187091), CD11b (550282, BD Biosciences), CD31 (MAB1398Z, Millipore), F4/80 (MCA497GA, Bio-Rad), and Ly6G (127602, BioLegend) overnight at 4°C. Primary antibodies were diluted 1:100 in Dako Protein Block. The sections were then incubated for 60 min at room temperature with Alexa Fluor 488-conjugated goat anti-rat (A11006, Thermo Fisher Scientific), Alexa Fluor 488-conjugated goat anti-rabbit (A11008, Thermo Fisher Scientific), and Alexa Fluor 568-conjugated goat anti-hamster (127-165-160, Iwai Chemicals) secondary antibodies, which were diluted at 1:1,000 in PBS. After three 10-min washes with PBS-T, slides were mounted with DAPI-Fluoromount-G (0100-20, Southern Biotech) and analyzed using a confocal microscope (STELLARIS 5, Leica).

For CD8 and IFN-γ staining, tissues were fixed with cold acetone for 10 min at −20°C and blocked by Dako Protein Block. PerCP-Cy5.5 anti-CD8 mAb (53-6.7, 100733, Biolegend) and Alexa Fluor 647 anti-mouse IFN-γ mAb (505816, Biolegend) were diluted 1:100 in Dako Protein Block and incubated for 60 min at room temperature. After two 10-min washes with PBS-T and a 10-min wash with PBS, slides were mounted with DAPI-Fluoromount-G (0100-20, Southern Biotech) and analyzed using a confocal microscope (STELLARIS 5, Leica). Excitation for DAPI, Alexa 488, Alexa 568, and Alexa 647 chromophores was provided by 405-, 488-, 568-, and 647-nm lasers, respectively, and a Plan-Apochromat oil objective (×63, NA 1.4). The Lightning mode (Leica) was used to generate deconvolved images. Microscope acquisitions were controlled by LAS X (v. 4.2.1) software from Leica. FL-IHC images, pMLKL, CD31-, CD11b-, F4/80-, Ly6G-, $CD8^-$, and IFN-γ positive areas were determined with Fiji software.[51] Each positive area was binarized and quantified using the Analyze Particle tool. 3 or 5 random fields per section were imaged.

Tumor xenograft and allograft models

Mice were anesthetized and injected subcutaneously with cancer cells suspended in 100 μL of PBS per mouse on day 0. In MIA-PaCa2 floating cell xenograft models, 5×10^6 MIA-PaCa2 floating cells at pH 7.4 and 6.8 were injected into 8-week-old female C.B-17/Icr-*scid*/*scid*Jcl mice. Tumors were isolated on day 21.

In FAM129C- or PIGR-overexpressing xenograft models, 1×10^7 control or FAM129C- or PIGR-overexpressing PANC1 MIA-PaCa2 cells were injected into 8-week-old female C.B-17/Icr-*scid*/*scid*Jcl mice. Tumors were isolated on day 31 (FAM129C-overexpressing PANC1 models), day 28 (FAM129C-overexpressing MIA-PaCa2 models), and day 19 (PIGR-overexpressing PANC1 models).

In FAM129C- or PIGR-overexpressing allograft models, 4×10^6 control or FAM129C- or PIGR-overexpressing murine pancreatic cancer cell line Pan02 or uterine cancer cell line HSML were injected into 8-week-old female C57BL/6 mice. Tumors were isolated on day 12 in Pan02 allograft models and on day 18 in HSML allograft models. In anti-PD-L1 and complement inhibitor treatment models, control group mice were treated with PBS from day 4, while PIGR-overexpressing groups were treated with either PBS from day 4, 10 mg/kg anti-mouse PD-L1 antibody (#A2115, Selleck) on days 4 and 7, 1 mg/kg complement inhibitor PMX53 (S6293, Selleck) daily from days 4–9, or a combination of anti-PD-L1 antibody and PMX53. All treatments were administered intraperitoneally. Tumors were isolated on day 9 after injection. Tumor growth was monitored every 2–3 days and analyzed using the Student's *t*-tests. To estimate the tumor volume, the long (L) and short (S) axes of the tumor were measured, and the tumor volume was calculated as $L \times S \times S/2$[56]

QUANTIFICATION AND STATISTICAL ANALYSIS

Survival analysis

We selected the top 10 enriched genes from the gRNA sequencing data (*MED12*, *TASA1*, *PBX4*, *MYO1A*, *PDGFRA*, *FAM129C*, *TADA2B*, *SUPT20H*, *CATSPERD*, and *NACC1*) and used them for Cox proportional hazards regression analysis. Models were constructed using RNA-seq expression profiles from TCGA via the Broad GDAC Firehose portal (http://gdac.broadinstitute.org/), including 705 glioma, 534 kidney renal clear cell carcinoma (KIRC), 263 sarcoma, 1100 breast invasive carcinoma (BRCA), 185 esophageal carcinoma, 95 rectum adenocarcinoma, and 509 thyroid carcinoma cases. In addition, microarray data of 102 pancreatic ductal adenocarcinoma (PAAD) patients were obtained from the Gene Expression Omnibus (GEO) dataset GEO: GSE21501.

To evaluate the prognostic relevance of cell-death-related genes, we performed Kaplan-Meier survival analyses of PAAD patients from the GEO dataset, stratified into high- and low-risk groups based on the expression of necroptotic (*RIPK1*, *RIPK3*, *MLKL*, *FADD*, *TNFR1*, *TRADD*), apoptotic (*BAX*, *BAK*, *CYCS*, *CASP9*, *CASP3*, *TP53*), ferroptotic (*GPX4*, *SLC7A11*, *ACSL4*, *ALOX15*, *TFRC*, *FTH1*), and pyroptotic (*CASP1*, *GSDMD*, *NLRP3*, *IL1B*, *CASP4*, *PYCARD*) genes. For each patient, a risk score was calculated using the linear predictor from the Cox proportional hazards model.

Pan-cancer analysis was based on the previous report.[52] In brief, the heatmap of DFI time and *MLKL*, *CASP3*, *GPX4*, and *GSDMD* expression was drawn by UNSC xena (https://xena.ucsc.edu) filtered "null" data. Pan-cancer analysis of *MLKL*, *CASP3*, *GPX4*, and *GSDMD* gene expression across pancreas and lung tumors available normal and tumor RNA-seq data was performed using the KM plot algorithm (https://kmplot.com/analysis/).[47,57] Then, the hazard ratio was drawn by GraphPad PRISM (ver. 10.5). The overall survivals of each gene from the top 10 genes of knockout screening were also determined using the TNM plot algorithm from pancreas

Please cite this article in press as: Hasegawa et al., Tolerance to extracellular acidic pH facilitates tumor plasticity, Cell Reports (2026), https://doi.org/10.1016/j.celrep.2026.117226

and lung tumors. The correlation of two selected genes was analyzed via the TNM plot "Correlation analysis" (https://tnmplot.com/analysis)[58] using RNA-seq data of TCGA choosing pancreatic adenocarcinoma.

Statistics

Subjective bias was minimized when allocating animals/samples to treatment using a randomization procedure. No data points were excluded or omitted from analysis. Plotted values are shown as means ± SEM throughout this study. Indicated p values were obtained using one-way analysis of variance (ANOVA) followed by Student-Newman-Keuls multiple comparisons for *post hoc* tests, paired Student's t tests, or Mann-Whitney U test. p values are denoted as $^{*}p < 0.05$; $^{**}p < 0.01$; $^{***}p < 0.001$; $^{****}p < 0.0001$; ns: not significant.